Magnetic responses of randomly depleted spin ladders

Arthur Lavarélo,[1,*] Guillaume Roux,[1,†] and Nicolas Laflorencie[2,‡]
[1]*Laboratoire de Physique Théorique et Modèles statistiques, Université Paris-Sud, CNRS, UMR8626, 91405 Orsay, France*
[2]*Laboratoire de Physique Théorique, Université de Toulouse, UPS, (IRSAMC), Toulouse, France*
(Received 24 July 2013; published 21 October 2013)

The magnetic responses of a spin-1/2 ladder doped with nonmagnetic impurities are studied combining both analytical and numerical methods. The regime where frustration induces incommensurability is taken into account. Several improvements are made on the results of the seminal work by Sigrist and Furusaki [M. Sigrist and A. Furusaki, J. Phys. Soc. Jpn. **65**, 2385 (1996)] and deviations from the Brillouin magnetization curve due to interactions are also analyzed. We first discuss the magnetic profile around a single impurity and the effective interactions between impurities within the bond-operator mean-field theory. The results are compared to density-matrix renormalization group calculations. In particular, these quantities are shown to be sensitive to the transition to the incommensurate regime. We then focus on the behavior of the zero-field susceptibility through an effective Curie constant. At zero temperature, we give doping-dependent corrections to the results of Sigrist and Furusaki on general bipartite lattices and compute exactly the distribution of ladder clusters due to chain breaking effects. Solving the effective model with exact diagonalization and quantum Monte Carlo simulations gives the temperature dependence of the Curie constant. Its high-temperature limit is understood within a random dimer model, while the low-temperature tail is compatible with a real-space renormalization group scenario. Interestingly, solving the full microscopic model does not show a plateau corresponding to the saturation of the impurities *in isotropic ladders*. The second magnetic response that is analyzed is the magnetic curve. Below fields of the order of the spin gap, the magnetization process is controlled by the physics of interacting impurity spins. The random dimer model is shown to capture the bulk of the curve, accounting for the deviation from a Brillouin behavior due to interactions. The effective model calculations agree rather well with density-matrix renormalization group calculations at zero temperature and with quantum Monte Carlo simulations at finite temperature. In all, the effect of incommensurability does not display a strong qualitative effect on both the magnetic susceptibility and the magnetic curve. Consequences for experiments on the $BiCu_2PO_6$ compound and other spin-gapped materials are briefly mentioned.

DOI: 10.1103/PhysRevB.88.134420 PACS number(s): 75.10.Kt, 75.40.Mg, 75.10.Jm, 75.10.Pq

I. INTRODUCTION

The presence of disorder and impurities in strongly correlated systems offers a good opportunity to better understand the role played by quantum fluctuations in such materials.[1] Either intrinsically present or explicitly added by doping, impurities in condensed matter systems can rarely be ignored, in particular when they induce new physics as compared to the disorder-free situation. Prominent examples are the Kondo effect,[2] Anderson localization,[3] dirty bosons physics in disordered superconductors,[4] impurities in magnetic semiconductors,[5] spin glasses,[6] etc.

In the context of antiferromagnetic (AF) Mott insulators, parent compounds of high-temperature superconducting cuprates for instance, spin ladder materials[7] have been shown to display very interesting features, in particular, when the number of legs is an even number. For example, a finite energy gap Δ_s appears in the excitation spectrum of two-leg AF spin-1/2 ladders,[8–10] as seen for instance in $SrCu_2O_3$.[11] Furthermore, defects in gapped ladders induce very interesting effects,[12–17] in particular, the apparition of effective gapless modes below the bare spin gap Δ_s. Having in mind that the ground state of a two-leg ladder displays short-range resonating valence-bond-like physics,[18] a nonmagnetic dopant is expected to break such a short-distance singlet, inducing a quasifree spin-$\frac{1}{2}$, strongly localized in the vicinity of the impurity. Interesting questions arise then when a finite concentration of impurities is introduced in a spin ladder, as studied in a large number of theoretical works.[19–33] Similar physics is also at play in other spin-gapped materials: spin-1 (Haldane) chains such as Y_2BaNiO_5,[34,35] or $PbNi1_2V_2O_8$,[36] spin-Peierls chains such as $CuGeO_3$[37–45] for instance. Indeed, a universal behavior can be observed for the impurity-induced three-dimensional ordering mechanism in such weakly coupled chains or ladder materials.[46]

Nevertheless, several aspects of impurity effects in ladder—and more generally spin gapped—materials remain to be explored in order to better understand and interpret experimental results. Regarding the effective pair-wise interaction between released moments, it is believed to remain nonfrustrated even when the underlying spin systems is frustrated,[47,48] but it is not clear to which extend such a result is robust when strong frustration leads to incommensurability,[49] as expected, for instance, in the ladder material $BiCu_2PO_6$.[16,50–56] A natural question then arises regarding which effective model is able to quantitatively describe the low-energy physics of randomly doped ladders. Indeed, it was believed since the seminal work of Sigrist and Furusaki[20] that a simple model of random (in sign and magnitude, reflecting the random locations of impurities in a ladder) nearest-neighbors couplings between effective spin-1/2 (describing impurity degrees of freedom) was able to correctly capture the low temperature physics of depleted ladders. This so-called random F-AF chain model[57–64] displays some universal behavior for various quantities such as uniform and staggered susceptibilities or the specific heat in the low-temperature regime, with an interesting large spin phase

occurring at very low temperature. However, in the context of depleted ladders, universality for such thermodynamic quantities has been first questioned using quantum Monte Carlo (QMC) simulations by Miyazaki and co-workers[27] where no clear signature of universal low-temperature scalings were found, in agreement with a more recent QMC study.[33]

Despite the large number of works devoted to such systems in the absence of external magnetic field, much less is known regarding finite field effects. Indeed, as recently reviewed by Giamarchi and co-workers,[65] applying a finite external field on gapped AF systems leads to the analog of a Bose-Einstein condensation (BEC) of magnetic excitations[66,67] (hard-core bosons triplets) when the field is sufficiently strong to close the spin gap Δ_s. Note that a true BEC is only expected for dimension $d > 2$, which occurs at low enough temperature below some energy scale controlled by three-dimensional couplings. Nevertheless, for low-d, a quasi-BEC is expected, as observed in ultracold atom physics.[68,69] In solid state physics, triplet BEC has been observed in several quantum magnetic compounds, such as coupled dimers $TlCuCl_3$,[70,71] frustrated bilayers $BaCuSi_2O_6$,[72] coupled Haldane chains in DTN,[73] and also spin ladder materials like $(C_5H_{12}N)_2CuBr_4$.[74–76]

However, when disorder is present in such spin gapped systems, a new phenomenology is expected with the interesting possibility to address Bose-Glass (BG) physics, as recently found in Br-doped $IPaCuCl_3$[77] or DTN[78] (see also Ref. 79 for a very recent review). While several issues remain unsolved regarding BG physics, e.g., for the excitation spectrum,[80–82] the case where disorder comes from ligand substitution seems easier to understand from a microscopic point of view. Indeed, such doping will essentially generate disorder in the AF couplings without inducing local moments. On the other hand, doping on the magnetic sites is expected to be more complicated as gapless states will populate the clean gap. Therefore the magnetic response will display nontrivial Brillouin-like behaviors in most of the experimentally relevant situations. Such cases have been studied theoretically by a few authors,[83–86] showing a rich physics and various scenarios that demand further analysis.

In this work, we focus on the two-leg ladder model to provide a systematic analysis of the physics of interacting impurities, building on both analytical and numerical arguments. In particular, we are interesting in the following issues: (i) the effective interaction between impurities for commensurate and incommensurate backgrounds, (ii) the low-energy emergence of large spins due to random signs in effective couplings in a realistic context including finite size effects due to chain breaking, (iii) the temperature scaling of the Curie constant of the uniform susceptibility, as obtained from both effective and realistic doped ladder models, and (iv) the deviations of the magnetic curve from the Brillouin response as a probe of the magnitude of interactions. The ladder model used throughout this study is the one studied in Refs. 53 and 87:

$$\begin{aligned}\mathcal{H} = \sum_{i=1}^{L} \; & J_1[\mathbf{S}_{i,1}\cdot\mathbf{S}_{i+1,1} + \mathbf{S}_{i,2}\cdot\mathbf{S}_{i+1,2}] \\ & + J_2[\mathbf{S}_{i,1}\cdot\mathbf{S}_{i+2,1} + \mathbf{S}_{i,2}\cdot\mathbf{S}_{i+2,2}] \\ & + J_\perp\,\mathbf{S}_{i,1}\cdot\mathbf{S}_{i,2}, \end{aligned} \tag{1}$$

where $\mathbf{S}_{i,j}$ is the spin-1/2 operator acting at site i of leg j and the J's are the magnitude of the various couplings, which are here taken to be antiferromagnetic ($J > 0$). In the rest of the paper, the only parameter coming with the presence of impurities is their concentration z. The doped microscopic model is numerically solved with two state-of-the-art methods: the density-matrix renormalization group (DMRG) technique[88] and the stochastic series expansion (SSE) quantum Monte Carlo technique.[89]

The paper is organized as follows. In a first part, we discuss in details the effective model describing two-body interactions between impurities. The resulting effective model is then compared to the solution of the microscopic model in the second part. The latter is dedicated to the study of the magnetization curve at field below the spin gap Δ_s, i.e., in the region dominated by the impurity spins response. This region is itself divide in two regimes: (i) the small-field regime $H \ll T$, featuring a temperature-dependent Curie constant $c(T)$, and (ii) the intermediate-field regime $T \lesssim H \lesssim \Delta_s$ displaying again deviations from Brillouin through an approximate power-law behavior. We do not investigate fields $H \gtrsim \Delta_s$ as the physics involves triplet bosons in a disordered medium, which is exciting but beyond the scope of the present manuscript.

II. EFFECTIVE INTERACTION BETWEEN IMPURITIES

In this first section, the emphasis is put on the quantitative analysis of the effective interaction between impurities from arguments similar to RKKY theory. This provides an effective Hamiltonian which couplings distribution is essential for understanding the magnetic responses. Previous works along this direction are found in Refs. 20 and 21.

A. Effective Hamiltonian

We start with the derivation of the low-energy effective Hamiltonian accounting for effective interactions between impurities. For a generic Heisenberg spin model with N spins, the clean Hamiltonian takes the general form

$$\mathcal{H}_{\text{clean}} = \frac{1}{2}\sum_{\mathbf{r},\mathbf{r}'} J_{\mathbf{r}-\mathbf{r}'}\mathbf{S}_{\mathbf{r}}\cdot\mathbf{S}_{\mathbf{r}'}, \tag{2}$$

where $J_{\mathbf{R}}$ are the microscopic couplings, which depend only on the relative distance $\mathbf{R} = \mathbf{r} - \mathbf{r}'$. We now consider that a few nonmagnetic impurities occupy sites $\mathbf{I}$ of the lattice. Then, the Hamiltonian reads

$$\mathcal{H} = \frac{1}{2}\sum_{\mathbf{r}\neq\mathbf{I}}\sum_{\mathbf{r}'\neq\mathbf{I}} J_{\mathbf{r}-\mathbf{r}'}\mathbf{S}_{\mathbf{r}}\cdot\mathbf{S}_{\mathbf{r}'}, \tag{3}$$

or $\mathcal{H} = \mathcal{H}_{\text{clean}} + \mathcal{H}_{\text{imp}}$, where

$$\mathcal{H}_{\text{imp}} = -\sum_{\mathbf{r}}\sum_{\mathbf{I}} J_{\mathbf{r}-\mathbf{I}}\mathbf{S}_{\mathbf{r}}\cdot\mathbf{S}_{\mathbf{I}}. \tag{4}$$

Notice that effective spins operators are introduced at sites $\mathbf{I}$ where the impurities live, while these sites are actually vacant. Hamiltonian (4) takes the form $\mathcal{H}_{\text{imp}} = -\sum_{\mathbf{r}}\mathbf{H}^{\text{eff}}_{\mathbf{r}}\cdot\mathbf{S}_{\mathbf{r}}$, in which $\mathbf{H}^{\text{eff}}_{\mathbf{r}} = \sum_{\mathbf{I}} J_{\mathbf{r}-\mathbf{I}}\mathbf{S}_{\mathbf{I}}$ is an effective magnetic field operator. Assuming the perturbation $\mathcal{H}_{\text{imp}}$ can be treated using linear

response theory, we may write the Fourier transform of $\mathbf{S_r}$:

$$\mathbf{S_k} \simeq \chi_{\mathbf{k}} \mathbf{H}^{\text{eff}}_{\mathbf{k}}, \tag{5}$$

with $\chi_{\mathbf{k}}$ is the static susceptibility at wave vector $\mathbf{k}$, and

$$\mathbf{H}^{\text{eff}}_{\mathbf{k}} = J_{\mathbf{k}} \sum_{\mathbf{I}} \mathbf{S_I} e^{i\mathbf{k}\cdot\mathbf{I}}. \tag{6}$$

One can thus write the perturbation $\mathcal{H}_{\text{imp}}$ as

$$\mathcal{H}_{\text{imp}} = \sum_{\mathbf{I},\mathbf{J}} J^{\text{eff}}_{\mathbf{I}-\mathbf{J}} \mathbf{S_I} \cdot \mathbf{S_J}, \tag{7}$$

where

$$J^{\text{eff}}_{\mathbf{R}} = -\sum_{\mathbf{k}} |J_{\mathbf{k}}|^2 \chi_{\mathbf{k}} e^{-i\mathbf{k}\cdot\mathbf{R}} \tag{8}$$

is the effective two-body interaction between impurities.

When the clean system possesses a spin gap associated to a spin correlation length ξ_{spin}, the susceptibility $\chi_{\mathbf{R}}$, and therefore the effective interaction $J^{\text{eff}}_{\mathbf{R}}$, decreases exponentially with the distance $\|\mathbf{R}\|$. For a sufficiently small impurity concentration z ($z \ll 1/\xi_{\text{spin}}$ in one dimension), effective interactions remain much smaller than the spin gap. At temperatures smaller than this gap, the clean part of the doped system can be considered to be in the ground state of $\mathcal{H}_{\text{clean}}$, while the impurities dynamics is governed by (7) in which one can take the zero-temperature behavior for the susceptibility $\chi_{\mathbf{k}}$.

B. Static susceptibility within the BOMF approximation

The static susceptibility of the ground state of (1) can be computed using the bond-order mean-field (BOMF) approximation[10,53] (see Appendix A). In the strong-coupling limit $J_\perp \gg J_1$, the spin gap is in the $k_y = \pi$ sector and the magnon branch is well separated from the two-magnons continuum. On can thus neglect the $k_y = 0$ contribution and keep only the single magnon one. The details of the calculations are given in Appendix A and show that the susceptibility displays the same singularities as the spin structure factor. In the large-$J_\perp$ regime, the result reads

$$\chi_{k,\pi} \simeq \frac{1}{4J_\perp + 8J_1 \cos k + 8J_2 \cos 2k}. \tag{9}$$

C. Magnetization profile induced by a single impurity

Before turning to the interaction between two impurities, it is first instructive to consider the magnetization pattern induced by a single impurity, which is also of interest for nuclear magnetic resonance (NMR) experiments. The impurity is located at site $\mathbf{I}_0$ and the corresponding effective magnetic field defined by (6) is simply given by $\mathbf{H}^{\text{eff}}_{\mathbf{r}} = J_{\mathbf{r}-\mathbf{I}_0} \mathbf{S}_{\mathbf{I}_0}$. The expectation value of the spin operator $\mathbf{S_r}$ is then given by linear response theory which, in Fourier transform, reads

$$\langle \mathbf{S_k} \rangle \simeq \chi_{\mathbf{k}} \langle \mathbf{H}^{\text{eff}}_{\mathbf{k}} \rangle. \tag{10}$$

This perturbative response is *a priori* valid far from the impurity. The magnetization profile in sector $S^z_{\text{tot}} = 1/2$ is then

$$\langle S^z_{\mathbf{I}_0+\mathbf{R}} \rangle \simeq \frac{1}{2\sqrt{2L}} \sum_{\mathbf{k}} e^{-i\mathbf{k}\cdot\mathbf{R}} \chi_{\mathbf{k}} J_{\mathbf{k}}, \tag{11}$$

where the general expression of the coupling of the frustrated ladder Hamiltonian (1) is

$$J_{\mathbf{k}} = \frac{1}{\sqrt{2L}} (2J_1 \cos k_x + 2J_2 \cos 2k_x + J_\perp \cos k_y). \tag{12}$$

After computing the integral limit of the sum (11) over the Brillouin zone, one obtains two different situations, depending on the behavior of the residues; in the commensurate regime $\frac{J_2}{J_1} < \frac{J_1}{4J_\perp}$, the profile is given by

$$\langle S^z_{x,y} \rangle \simeq \frac{1}{8}(-1)^{x+y} \left\{ \frac{e^{-x/\xi^+_{\text{spin}}}}{\sinh(1/\xi^+_{\text{spin}}) P'[-\cosh(1/\xi^+_{\text{spin}})]} + \frac{e^{-x/\xi^-_{\text{spin}}}}{\sinh(1/\xi^-_{\text{spin}}) P'[-\cosh(1/\xi^-_{\text{spin}})]} \right\}, \tag{13}$$

where $\xi^\pm_{\text{spin}}$ are the spin correlation lengths defined in Eq. (A8) and $P'(X)$ is the derivative of the polynomial $P(X)$ defined in Eq. (A4). In the incommensurate regime $\frac{J_2}{J_1} > \frac{J_1}{4J_\perp}$, one has

$$\langle S^z_{x,y} \rangle \simeq \frac{1}{4}(-1)^y e^{-x/\xi_{\text{spin}}} \times \Im \left\{ \frac{e^{iqx}}{\sin\left(q + i\xi^{-1}_{\text{spin}}\right) P'\left[\cos\left(q + i\xi^{-1}_{\text{spin}}\right)\right]} \right\}, \tag{14}$$

where q and ξ_{spin} are defined by Eqs. (A10) and (A11). Notice that there is no unknown constant in these expressions.

The key point of this result is that the transition from commensurate to incommensurate correlations induces a discontinuity in the features of the magnetization profile, which will show up in the effective interaction too. Indeed, at each side of the transition, both residues diverge but their sum tends to zero. Notice that exactly at the transition, the denominator factorizes, having a single pole of order 2 for which the residue is zero, corresponding to $\langle S^z_{x,y} \rangle = 0$. On the contrary, the amplitude of the magnetization $\langle S^z_{x,y} \rangle$ goes to $+\infty$ at each side of the transition, but this does not mean that the magnetization profile diverges at short distance. Of course, $\langle S^z_{x,y} \rangle$ remains always bound by $1/2$. However, the fact that the amplitude of the asymptotic behavior diverges which makes the perturbative analysis of the linear response fail.

On Fig. 1, we compare the magnetization profile in the sector $S^z_{\text{tot}} = 1/2$ obtained by DMRG to the mean-field predictions. In practice, expressions (13) and (14) provide good estimates of the behaviors, but it is preferable to fit the magnetization profiles using the following ansatz:

$$\langle S^z_{x,y} \rangle = C(-1)^{x+y+1} e^{-x/\xi_{\text{spin}}}, \tag{15}$$

in the commensurate regime, and

$$\langle S^z_{x,y} \rangle = C(-1)^{y+1} e^{-x/\xi_{\text{spin}}} \cos(qx + \phi), \tag{16}$$

in the incommensurate one. Remarkably, except near the onset of incommensurability where the amplitude diverges, these expressions remain correct at small distances, down to $x = 1$. In NMR experiments, an incommensurate q would give a narrowing of the peak with respect to the commensurate case with the same ξ_{spin} since the magnetization will display smaller values even close to the impurity.

These profiles give a simple way to numerically access the fit parameters and compare them to BOMF predictions.

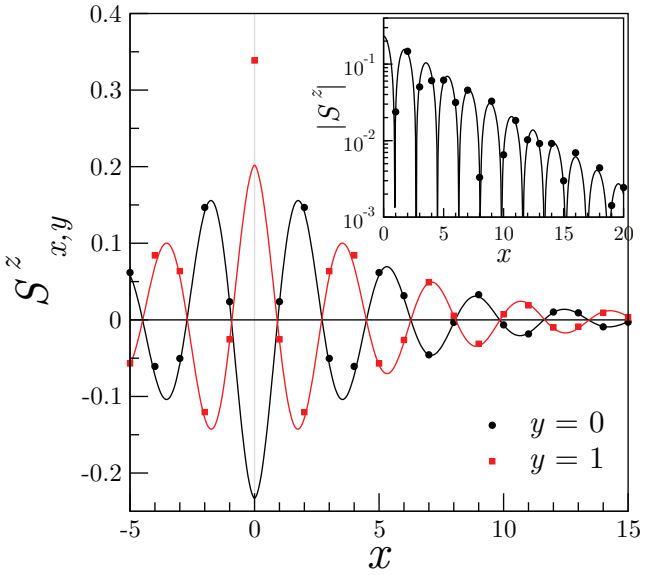

FIG. 1. (Color online) Magnetization profile in sector $S^z_{\rm tot} = 1/2$ induced by a nonmagnetic impurity at site (0,0), for an isotropic ladder ($J_\perp = J_1$) with $J_2 = J_1$. The incommensurate regime displays oscillations at wave vector q. The fit is done using (16).

Indeed, the values of $\xi_{\rm spin}$ and q extracted from the magnetization profiles agree qualitatively well with the mean-field predictions, as shown on Fig. 2. In particular, we checked that the amplitude C possesses a maximum close to the transition from commensurate to incommensurate. Physically, these calculations provide an explicit illustration of the fact that the impurity generates a spinon that is confined close to it through an effective attractive potential acting over a typical length scale $\xi_{\rm spin}$.

Last, we stress that there is a qualitative difference between the magnetization profile and the spin correlation function (see Appendix A for discussion of spin correlations in the model). One does not expect a power-law correction in the decay of the magnetization. This is clearly visible on Fig. 3 where fitting the envelope using $e^{-x/\xi_{\rm spin}}/x^\eta$ gives an exponent $\eta \simeq 0$, while the exponent found for the fit of the correlations is rather $\eta \simeq 1/2$, as expected from the usual

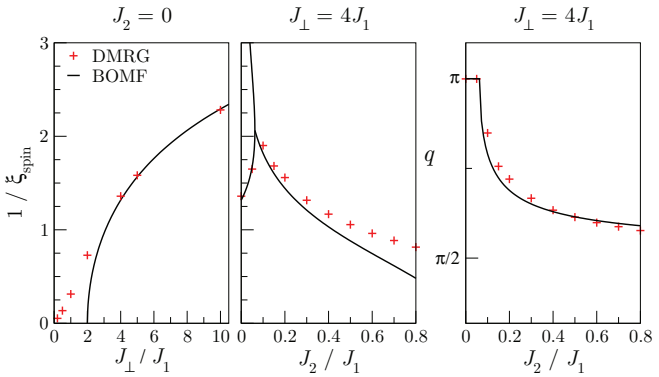

FIG. 2. (Color online) Correlation length $\xi_{\rm spin}$ and wave vector q extracted from the magnetization profile induced by a single impurity. DMRG results are compared to BOMF predictions in the large-$J_\perp$ regime.

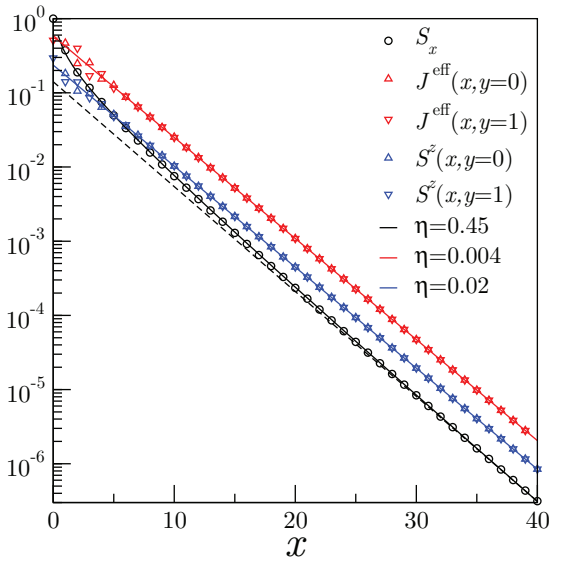

FIG. 3. (Color online) Magnetization profile in sector $S^z_{\rm tot} = 1/2$ induced by a nonmagnetic impurity at site (0,0), for an isotropic ladder ($J_\perp = J_1$) for $J_2 = 0$ in the commensurate regime. The decay of the magnetization profile and effective interaction between two impurities are compared to the decay of spin correlations. These three quantities display the same length scale $\xi_{\rm spin}$ in the exponential. Yet, only correlations display a power-law correction (see Appendix A).

arguments recalled in Appendix A. These quantitative results on the magnetization profiles and their sensitivity to the commensurate-incommensurate transition share similarities with those on the effective interaction between impurities, which we now discuss.

D. Effective interaction between impurities

1. Long-distance behavior

Within the BOMF approximation, valid in the strong-coupling limit, the effective interaction between impurities of Eq. (8) takes the following form in the thermodynamical limit:

$$J^{\rm eff}_{x,y} \simeq \frac{J_\perp}{8}(-1)^{y+1}\frac{1}{2\pi}\int_0^{2\pi}\frac{Q^2(\cos k)}{P(\cos k)}e^{ikx}dk, \qquad (17)$$

where Q is the polynom

$$Q(X) = 1 + 2\frac{J_2}{J_\perp} - 2\frac{J_1}{J_\perp}X - 4\frac{J_2}{J_\perp}X^2. \qquad (18)$$

As for the magnetization profile, one can evaluate the integral using the residue theorem to obtain two cases: in the commensurate regime, one has

$$J^{\rm eff}_{x,y} \simeq \frac{1}{8}(-1)^{x+y+1} \times \left\{ \frac{Q^2[-\cosh(1/\xi^+_{\rm spin})]}{\sinh(1/\xi^+_{\rm spin})P'[-\cosh(1/\xi^+_{\rm spin})]}e^{-x/\xi^+_{\rm spin}} + \frac{Q^2[-\cosh(1/\xi^-_{\rm spin})]}{\sinh(1/\xi^-_{\rm spin})P'[-\cosh(1/\xi^-_{\rm spin})]}e^{-x/\xi^-_{\rm spin}} \right\}, \qquad (19)$$

while in the incommensurate regime, one has

$$J^{\rm eff}_{x,y} \simeq \frac{1}{4}(-1)^{y+1} e^{-x/\xi_{\rm spin}} \times \Im\left\{ \frac{Q^2\left[\cos\left(q+i\xi^{-1}_{\rm spin}\right)\right]}{\sin\left(q+i\xi^{-1}_{\rm spin}\right) P'\left[\cos\left(q+i\xi^{-1}_{\rm spin}\right)\right]} e^{iqx} \right\}. \quad (20)$$

Similarly to the magnetization profile, the amplitude of $J^{\rm eff}_{x,y}$ diverges close to the transition between the two regimes but is strictly zero at the transition point. This divergence does not mean that the effective interaction gets stronger but rather that the applicability of the long-distance result is limited to large distances. The effective interaction remains always bonded by the maximum of J_1 and J_2 (see short distances behavior hereafter).

Further, no power-law corrections are expected in this quantity, contrarily to what is commonly proposed.[20,84] Yet, this result is valid in the strong-coupling limit and we observe that it remains correct down to the isotropic ladder regime. In the weak-coupling limit, it is possible to have power-law or logarithmic corrections but we have not studied this case quantitatively.

Numerically, we compute the effective interaction using DMRG by targeting the lowest energies in the singlet and triplet sectors. We assume that the lowest triplet excitation is due to the interaction between the two impurities (the spin gap is large enough in this system) so that one can use the relation

$$J^{\rm eff} = E_{S_{\rm tot}=1} - E_{S_{\rm tot}=0}. \quad (21)$$

Only the total $S^z_{\rm tot}$ is fixed in DMRG calculations. Thus, since the triplet sector has a contribution for $S^z_{\rm tot}=0$, one accesses to the amplitude $|J^{\rm eff}|$ from the energy difference of the first two energies in this sector. In order to get the sign of $J^{\rm eff}$, one compares the obtained energies in sector $S^z_{\rm tot}=0$ with the lowest in sector $S^z_{\rm tot}=1$. On Fig. 4, we fit the curves using the function

$$J^{\rm eff}_{x,y} = J_0(-1)^{y+1} e^{-x/\xi_{\rm spin}} \cos(qx+\phi), \quad (22)$$

where $q=\pi$ and $\phi=0$ in the commensurate regime. As expected, the wave vector q and length scale $\xi_{\rm spin}$ exactly

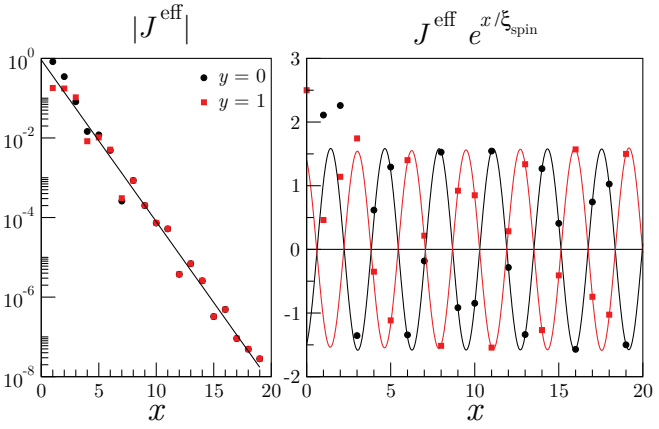

FIG. 4. (Color online) Behavior of the effective interaction $J^{\rm eff}_{x,y}$ between to impurities as a function of their relative distance for $J_\perp = 3J_1$ and $J_2 = J_1/2$. DMRG results (symbols) are fitted using the expression (22).

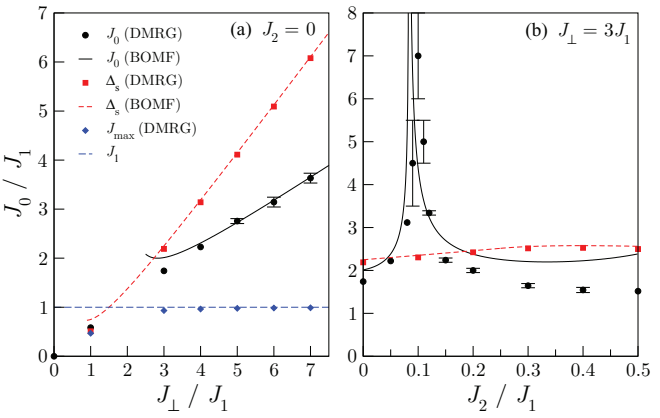

FIG. 5. (Color online) Amplitude J_0 of the effective interaction. (a) Evolution without frustration ($J_2=0$) for increasing coupling $J_\perp/J_1$. Comparison with other energy scales is given: the mean antiferromagnetic couplings J_+ and the maximum value of the effective interaction couplings $J_{\rm max}$. (b) Evolution in the strong-coupling regime $J_\perp = 3J_1$ for increasing frustration J_2/J_1, showing the divergence at the transition to the incommensurate regime.

correspond to the ones of the magnetization profile and correlations function. The behavior of the amplitude J_0 is not quantitatively predicted by the BOMF theory as, for instance, the behavior of $\xi_{\rm spin}$ is not in perfect agreement, due to the approximations made in the BOMF. Still, as one sees in Fig. 5, the amplitude J_0 displays a sharp increase in the vicinity of the commensurate-incommensurate transition, reminiscent from the divergence expected in Eqs. (19) and (20).

2. *Short-distance behavior*

The short distances effective interactions computed with DMRG, and displayed on Fig. 4, do not follow the prescription (22). In fact, although linear response theory fails at these distances, one can guess the sign and magnitude of $J^{\rm eff}$ by looking at each configuration (see Fig. 6). The first thing

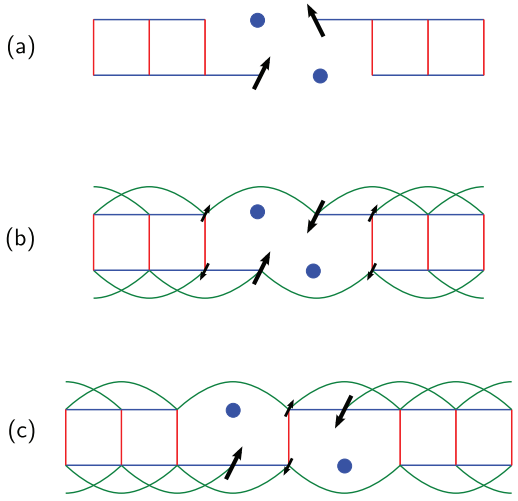

FIG. 6. (Color online) Impurities configurations for which the effective interaction does not have the sign expected from relation (22): (a) $\mathbf{r}=(1,1)$ with $J_2=0$, (b) $\mathbf{r}=(1,1)$ with $J_2\neq 0$, and (c) $\mathbf{r}=(2,1)$ with $J_2\neq 0$.

to notice is that a configuration with impurities on the same rung breaks the ladder and the elementary excitation is then a magnon in the largest piece which energy cost is slightly larger than the spin gap. Such effect does not enter in the effective model since no spin-1/2 is located at the vicinity of an impurity in that case.

Without frustration ($J_2 = 0$), the effective interaction oscillates at $\mathbf{k} = (\pi,\pi)$, even at short distances, except when $\mathbf{r} = (1,1)$ for which the effective coupling is almost zero within DMRG accuracy. Indeed, we observe in Fig. 6(a) that this configuration breaks the ladder. Two spinons are then generated on disconnected fragments and behave independently, making the triplet and singlet states degenerate and the effective interaction equal to zero. The largest value of the effective interaction, which we write $J_{\max}$ in the following, is obtained when two impurities are neighbor on the same chain. The magnitude is then controlled by J_1 and shown on Fig. 5(a).

In the presence of frustration, the configuration with $\mathbf{r} = (1,1)$ no longer breaks the ladder. Figure 6(b) shows that spinons freed by the impurities should antialign due to J_2, as for the configuration with $\mathbf{r} = (2,1)$ sketched in Fig. 6(c). In both cases, the corresponding effective interaction is expected to be antiferromagnetic (positive), in agreement with the DMRG result of Fig. 4. If J_2 is larger than J_1, it typically sets the scale of the maximum coupling $J_{\max}$ in the effective interaction.

Last, one can recall that two-body interactions is just an approximation and that terms involving more than two partners should be included to improve the comparison with *ab initio* calculations involving many impurities. The validity of two-body interaction has been discussed in Ref. 25 to which we refer to for further details on this question.

E. Distribution of couplings between impurities

We here discuss the nature of the couplings distribution $P(J)$ resulting from doping the ladder and which is a central quantity for the understanding of the magnetic responses. We use the following notation from now on: N is the total number of sites, $L = N/2$ the length of the ladder, N_i the number of impurities, and $z = N_i/N$ the impurities concentration or doping. The latter corresponds to the probability for a site to be occupied by an impurity. The lattice spacing is taken to be one in both directions. The relative distance between two points on the ladder is written as $\mathbf{r} = (n_x,n_y)$ with $n_x = 0,1,2,\ldots$ and $n_y = 0,1$.

Consider impurities that are randomly distributed on the ladder. The probability p_{n_x,n_y} of having a distance $\mathbf{r}$ between two impurities is given by a geometric law:

$$p_{n_x,n_y} = z(1-z)^{2n_x+n_y-1} \quad \text{for} \quad n_x + n_y > 0. \tag{23}$$

To understand this formula, one can scan all intermediate sites between the impurities following a zigzag path. Thus, within the ladder geometry, which has the peculiarity to differ from a chain because of the possibility to put two impurities on the same rung (case with $n_x = 0$ and $n_y = 1$), we have the following results for the mean longitudinal and transverse distances:

$$\bar{x} = \frac{1}{z}\left(\frac{1-z}{2-z}\right), \tag{24}$$

$$\bar{y} = \frac{1}{2-z}. \tag{25}$$

One recovers the intuitive behaviors $\bar{y} \simeq 1/2$ and $\bar{x} = 1/(2z)$ in the dilute limit $z \ll 1$. Thus, in this limit, the typical average distance d between impurities, as if they were on a chain, is given by the effective doping $z' = 2z$ as $d \simeq 1/z'$ and one has to keep in mind the presence of this factor two in qualitative reasoning.

To obtain the distribution of couplings, we use for analytical calculations the simplified and generic relation

$$J(\mathbf{r}) = J_0(-1)^{y+1}\cos(qx+\phi)e^{-x/\xi} \tag{26}$$

with q a dimensionless wave vector, which accounts for a possible incommensurability and ξ the spin correlation length (in a shortened notation), ϕ a phase shift, and J_0 an energy scale. Their typical behavior with microscopic parameters was discussed in the previous sections. Formally, one obtains the distribution of couplings using the definition

$$p(J) = \iint d\mathbf{r}\; p(\mathbf{r})\delta(J - J(\mathbf{r})) \tag{27}$$

and use for the discrete case

$$p(\mathbf{r}) = \sum_{(n_x,n_y)} p_{n_x,n_y}\delta(x-n_x)\delta(y-n_y). \tag{28}$$

As we will see, the magnetic curve will be deeply connected to the coupling repartition function that we denote by

$$R(J) = \int_{-\infty}^{J} P(J')dJ'. \tag{29}$$

We also introduce the repartition function of antiferromagnetic couplings only:

$$R_+(J) = \frac{R(J) - R(0)}{1 - R(0)} \quad \text{for} \quad J > 0. \tag{30}$$

Indeed, negative Js corresponding to ferromagnetic couplings will yield polarized impurities as soon as the field is turn on. A correct way of defining an energy scale corresponding to a magnetic field in the problem is thus to average only the positive Js. Then, we take the following definition

$$J_+ = \frac{\int_0^\infty J\,P(J)dJ}{\int_0^\infty P(J)dJ} \tag{31}$$

for the typical energy scale of the antiferromagnetic couplings.

1. Commensurate case

In this case, the interaction is purely antiferromagnetic corresponding to $q = \pi$. Changing variables is done using

$$\delta(J - J(\mathbf{r})) = \frac{\xi}{|J|}\delta(x - n(J)),$$

with $n(J) = \xi\ln(J_0/|J|)$.

a. Continuous distribution. We first consider the most elementary situation where $p(\mathbf{r})$ is approximated by a continuous

function, which requires $z \ll 1$ and $\xi \gg 1$ with fixed $z\xi$. Then, what enters in the distance probability is the effective chain doping z', giving the exponential law $p(x) \simeq z' e^{-z'x}$. The calculation yields a symmetric power-law distribution

$$p(J) = \frac{z\xi}{J_0} \left(\frac{J_0}{|J|} \right)^{1-2z\xi} \tag{32}$$

for $J \in [-J_0, J_0]$, featuring the exponent $1 - 2z\xi$. The corresponding repartition function reads

$$R(J) = \frac{1}{2} \left[1 + \mathrm{Sign}(J) \left(\frac{|J|}{J_0} \right)^{2z\xi} \right]. \tag{33}$$

The energy scale J_+ takes the simple form

$$J_+ = \frac{2z\xi}{1 + 2z\xi} J_0. \tag{34}$$

A similar expression has been used to interpret experiments with 3D effects.[46] Here, the effective volume of the interaction boils down to 2ξ.

b. Exact distribution and lattice effects. The continuous distribution ansatz is not justified for systems with very short correlation length such as the isotropic ladder. We here carry out the calculation in the discrete case to obtain the exact formula that can be compared to numerical histograms of the couplings used in numerical simulations. We have

$$p(J) = \sum_n P(J) \delta(n - n(J))$$

and

$$P(J) = \frac{z\xi}{(1-z)J_0} \left(\frac{J_0}{|J|} \right)^{1+2\xi \ln(1-z)}$$

for $J \in [-J_0, J_0]$. One recovers the result of the continuous approximation under its assumption. In particular, one can see that lattice effects decouple the effect of the correlation length and of the impurity concentration, i.e., the exponent is not a function of $z\xi$ only, but a function of both z and ξ, which makes the results not so universal. Last, we notice that the distribution becomes flat for the particular value

$$z^* = 1 - e^{-1/(2\xi)}, \tag{35}$$

and we will see that this can have consequences on the shape of the magnetic curve.

For the typical energy scale J_+, the exact result is computed by directly summing upon the (n_x, n_y) and one obtains

$$J_+ = \frac{1 - (1-z)^4}{2 - z} \frac{1 + (1-z)e^{-1/\xi}}{1 - (1-z)^4 e^{-2/\xi}} J_0. \tag{36}$$

Here again, one can check that (34) is recovered provided $\xi \gg 1$ and $z \ll 1$ while keeping ξz finite. Otherwise, deviations from (34) occur at all doping. In particular, the low-doping regime $z \ll 1$ at fixed ξ is

$$\frac{J_+}{2J_0 z} \simeq \frac{1 + e^{-1/\xi}}{1 - e^{-2/\xi}} = \xi \left(1 - \frac{1}{2\xi} + \cdots \right). \tag{37}$$

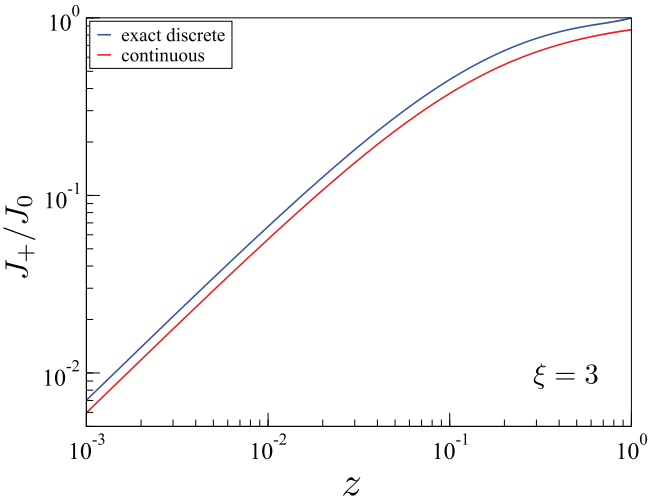

FIG. 7. (Color online) Typical energy scale of the coupling distribution as a function of doping z for a realistic value of the correlation length $\xi = 3$. The continuous approximation result is compared to the exact discrete result, showing lattice effects discussed in the text.

These lattice effects are illustrated in Fig. 7 for a realistic case with $\xi = 3$, which is characteristic of the isotropic ladder limit.

2. *Incommensurate case and numerical sampling*

In this case, the $J(\mathbf{r})$ function is not bijective, which changes qualitatively the distribution of the J's. The presence of the cosine significantly lowers the weight of the largest J's, while the smallest J's will see their weight increase. Second, in the presence of fractional q/π, commensurate effects happen while an irrational q/π has qualitatively the behavior of a true quasiperiodic signal. In particular, for rational q/π and $\phi = 0$, a fraction of couplings can be zero. Yet this situation is unphysical for the model under consideration whose generic case is a nonzero phase shift and irrational q/π.

In order to illustrate the typical behavior of the repartition function in the commensurate and incommensurate regimes, we have sampled numerically the distribution of couplings. Results are gathered in Fig. 8. The essential features are the following: (i) up to discrete effect, the exponent $2z\xi$ in Eq. (33) captures well the power-law in the commensurate case; (ii) for irrational q/π, the repartition function is qualitatively very close to the commensurate case, with a similar exponent, and up to the weight redistribution towards lower J, which translates into a smaller energy scale J_+. (iii) For rational q/π and $\phi = 0$, plateaus appear at $1/4$ and $1/5$ in the figure, corresponding the many zero couplings, together with cusps in J_+. Yet, the latter situation being unphysical, the main conclusion is that incommensurability hardly affects the coupling distribution. The fact that frustration, throughout incommensurability, only lowers the energy scale J_+ but hardly affects the distribution is essential to understand that frustration will have only minor effects on the local magnetic responses studied in the next sections.

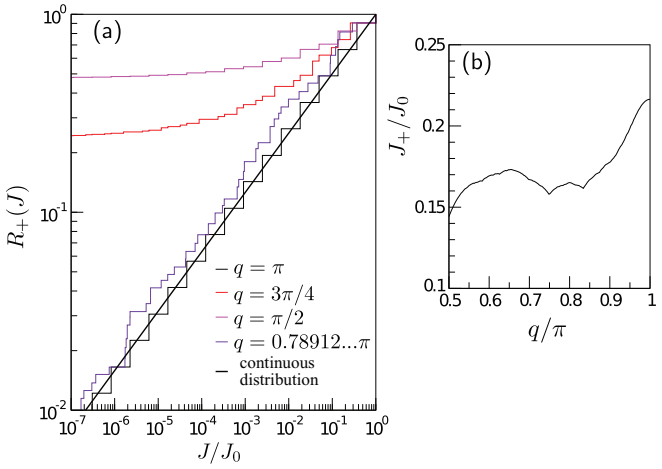

FIG. 8. (Color online) (a) Repartition function of positive couplings $R_+(J)$ for $z = 0.05$ and $\xi = 3$ with $\phi = 0$. (b) Energy scale J_+ vs the incommensurate wave vector q.

III. EXACT ZERO-TEMPERATURE RESULTS ON A BIPARTITE LATTICE: AVERAGED SPIN AND CURIE CONSTANT

In this section, we improve on the work of Sigrist and Furusaki[20] for the calculation of the averaged total spin and zero-temperature Curie constant of a doped system on a bipartite lattice. The results that are obtained are more general than for the special case of a ladder, and can be useful in checking numerical simulations and understanding finite-size corrections.

A. Total spin distribution

We assume a finite size sample containing N sites and doped with $N_i = zN$ impurities, where z is the impurity concentration which is fixed. The impurities are assumed not to break the lattice into disconnected sublattices (see discussion Sec. III C). On a bipartite lattice, with two sublattices A and B, which have the same number of sites $N/2$, applying Marshall's theorem yields that the total spin S of a given impurity configuration reads

$$S = \tfrac{1}{2}|N_{i,A} - N_{i,B}| = \tfrac{1}{2}|2N_{i,A} - N_i|, \tag{38}$$

where $N_{i,A}$ (respectively $N_{i,B}$) is the number of impurities on sublattice A (respectively B). The probability of having a configuration with $N_{i,A}$ impurities on sublattice A is qualitatively similar to the result on a ferro-antiferromagnetic (F-AF) chain,[61] and given by

$$P(N_{i,A}) = \frac{\binom{N/2}{N_{i,A}}\binom{N/2}{N_i - N_{i,A}}}{\binom{N}{N_i}}. \tag{39}$$

Then, the probability of having a total spin S on a sample is

$$P_{z,N_i}(S) = \frac{\binom{N/2}{\frac{N_i}{2}+S}\binom{N/2}{\frac{N_i}{2}-S}}{\binom{N}{N_i}}(2 - \delta_{S,0}), \tag{40}$$

where $S \in [0, N_i/2]$. This result is exact and can be used to compute numerically the mean total spin and the Curie constant. For large N_i and fixed z, according to the central limit theorem, $P_{z,N_i}(S)$ converges towards a Gaussian. A saddle-point calculation gives the asymptotic behavior

$$P_{z,N_i}(S) \simeq \frac{2}{\sqrt{2\pi\sigma_S^2}} e^{-S^2/2\sigma_S^2} \tag{41}$$

of variance $\sigma_S^2 = \frac{N_i}{4}(1 - z)$.

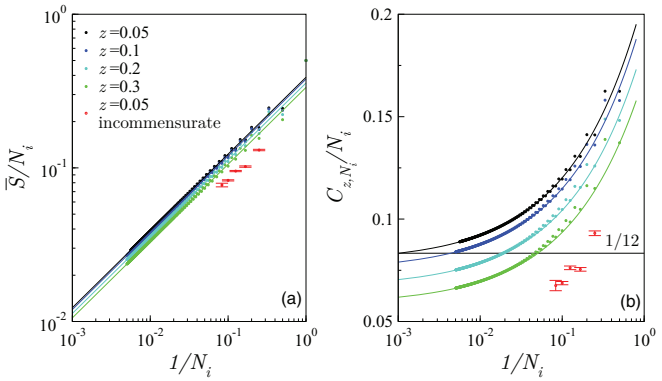

FIG. 9. (Color online) (a) Finite-size scaling of the average total spin $\overline{S}$, for four different doping z, obtained from exact calculations (points) and compared to Eq. (42). (b) The finite-size correction of the zero-temperature Curie constant, compared to Eq. (44). The 1/12 line shows the usually admitted result. The incommensurate case corresponds to an isotropic ladder with $J_2 = 0.8J_1$.

B. Total spin and Curie constant

One then obtains the average spin and the average square-spin in the $N \to \infty$ limit as

$$\overline{S} \simeq \sqrt{\frac{1-z}{2\pi}}\sqrt{N_i} \quad \text{and} \quad \overline{S^2} \simeq \frac{1-z}{4}N_i. \tag{42}$$

The total zero-temperature Curie constant matches exactly:

$$C_{z,N_i} = \overline{\langle \hat{S}_z^2 \rangle} = \frac{\overline{S(S+1)}}{3}. \tag{43}$$

From (42), we obtain the following asymptotic behavior:

$$C_{z,N_i} = \frac{N_i}{12}(1-z)\left[1 + \sqrt{\frac{8}{\pi(1-z)}}N_i^{-1/2}\right]. \tag{44}$$

These asymptotic results are compared to numerical calculations using the exact distribution on Fig. 9. In the thermodynamical limit $N_i \gg 1$, we thus find that the Curie constant *per impurity* is $(1 - z)/12$ at $T = 0$, while the Curie constant *per spin* is $z/12$. Notice that one can also compute exactly the average of the squared spin:

$$\overline{S^2} = \left[\frac{N_i^2}{4}\binom{N}{N_i} - N(N_i-1)\binom{N-1}{N_i-1} + N(N-1)\binom{N-2}{N_i-2}\right] \Big/ \binom{N}{N_i},$$

which is useful to crosscheck the statistical convergence of averaging over samples, but we did not manage to compute exactly $\overline{S}$.

These results remain correct in the commensurate regime because the effective model is still unfrustrated, but in the

incommensurate regime, expressions (42) are not valid anymore. The total spin and Curie constant at zero temperature can be computed from exact diagonalization (ED) on the effective model using the exact couplings extracted from DMRG data. The results for a frustrated isotropic ladder in the incommensurate regime are shown on Fig. 9. The frustration induced by the incommensurability yields a appreciable reduction of both the total spin and the Curie constant. Note that this reduction is essentially due to the short distance behavior of the effective interaction, hence the necessity to use the exact effective couplings computed in DMRG rather than the asymptotic law (22).

The doping dependence of the prefactors and finite-size corrections were missed in previous work. They originate from the dilution of the lattice. They actually play a crucial role in the quantitative understanding of the numerics that usually work with a restricted number of impurities. Last, the precise value at finite-size is essential in extracting the low-temperature exponent, as we will see in the next section.

C. Chain breaking effects on the ladder

1. Percolation scenario in the general case

Results in Eqs. (42) and (44) are exact assuming that there is a fully connected cluster containing N_i impurities over $N = N_i/z$ sites. Of course, the network can be disconnected in many subclusters by the presence of impurities. Then, each cluster, which is a finite size system, will eventually contribute to $\bar{S}$ and C in the thermodynamical limit, which was pointed out by Sigrist and Furusaki who computed an evaluation of the correction in the ladder case.[20] Thus we expect that, in general, $\bar{S}/N_i \neq 0$ in the thermodynamical and that C is not exactly given by (44). Lastly, it has been proposed in Ref. 20 that these breaks provide a natural cut in the length scale (and an energy scale), which should affect the behavior of the correlations. This was confirmed numerically in Ref. 33 in which results on depleted two-leg ladders are consistent with an upper bound of the order of z^{-2} reached for very low temperatures.

The probability and size distribution of these clusters are governed by percolation theory. The percolation transition distinguishes two main regimes: (i) there exist an infinite cluster of sites below a certain critical doping z_c, (ii) for $z > z_c$, only finite-size clusters exist and their size distribution is typically exponential, associated with a mean cluster size that will be denoted by $\bar{\ell}$ in the following. At the critical doping $z = z_c$, there is still an infinite cluster and scaling is expected for the mean cluster size. The value of z_c is very sensitive to dimensionality and connectivity of the lattice. These percolation regimes induce important finite size effects and are essential for experiments and numerical simulations. On a chain, it is clear that $z_c = 0$, i.e., any finite doping will break the lattice and the mean cluster size is easily related to the doping $\bar{\ell} \sim 1/z$. On a ladder, the situation is similar in the sense that any finite doping breaks the lattice into subclusters. This chain breaking effects have been shown to have quantitative results on the magnetic response of doped chains.[90] Yet, computing $\bar{\ell}$ in the case of ladder is not trivial and the remaining clusters are themselves doped with various concentration of impurities which makes the predictions more involved. We give below an exact discussion of the cluster sizes in the ladder and apply the results to the chain breaking effects on ladders.

2. Cluster distribution for the unfrustrated ladder network

We consider a ladder with nearest-neighbor only. Connectivity of the network is broken if (i) two impurities fall on the same rung, or (ii) two impurities fall on diagonal positions on a plaquette [see Fig. 6(a)]. If $(x,0)$ is the impurity position, there are three positions at which a second impurity can break the ladder: $(x-1,1)$, $(x,1)$, and $(x+1,1)$. Occupying a site with an impurity has a probability z. In the diluted limit $z \ll 1$, the density of cuts is then $3z^2$ and the corresponding mean cluster size is given by $\bar{\ell} \simeq 1/3z^2$ (the factor 3 was missing in Ref. 20). Notice that in the presence of frustration, chain-breaking requires at least four neighboring impurities, which would make a different scaling $\bar{\ell} \sim 1/z^4$. For large enough distances, breaks are uncorrelated so a fair description of the distribution law is that of a Poissonian process

$$\rho(\ell) \simeq \zeta e^{-\zeta \ell}, \tag{45}$$

with $\zeta = 1/\bar{\ell} \simeq 3z^2$ in the diluted and continuum limit.

An exact calculation of the cluster sizes distribution is carried out in Appendix C and supports this phenomenological approach. The exact distribution reaches very quickly an asymptotic behavior given by a geometric law

$$\rho(\ell) \simeq \zeta(1-\zeta)^{\ell-1} \tag{46}$$

of parameter

$$\zeta = \tfrac{1}{2}[1+z-(1-z)\sqrt{1+4z(1-z)}] \underset{z\ll 1}{\simeq} 3z^2. \tag{47}$$

Consequently, one recovers (45) in the continuum limit and $\bar{\ell} = 1/\zeta$. In particular, this provides finite-z corrections to the $1/z^2$ scaling, which turn out to be quantitative even for a few percent doping as we see now.

3. Consequences for the averaged spin and Curie constant

Averaging the total spin and Curie constant over clusters is not trivial since the doping of each cluster can now be distributed between zero and approximately 1/2. To handle a correct estimate, one would have to average using the joint distribution of cluster sizes and doping. We give below a rough estimate that consists in assuming a fix doping z for all cluster and averaging only over cluster sizes ℓ using $N_i = 2\ell z$. Neglecting the doping fluctuations should yield a good approximation in the diluted limit where cluster sizes diverge. Averaging Eq. (42) is performed using

$$\overline{\overline{S_{\rm tot}}} \simeq \sum_{\ell=1}^{+\infty} \rho(\ell)\sqrt{\frac{z}{\pi}(1-z)\ell} \quad \text{and} \quad \overline{\overline{S_{\rm tot}^2}} \simeq \sum_{\ell=1}^{+\infty} \rho(\ell)\frac{z}{2}(1-z)\ell.$$

Using the approximate law (46) for the size distribution and a continuous approximation for the average spin, we get

$$\overline{\overline{S_{\rm tot}}} \simeq \frac{1}{2}\sqrt{\frac{z}{\zeta}(1-z)} \quad \text{and} \quad \overline{\overline{S_{\rm tot}^2}} \simeq \frac{z}{2\zeta}(1-z)(1-\zeta). \tag{48}$$

To obtain the density of spin and Curie constant, one has to multiply them by the clusters density ζ. The mean spin density $\bar{s} = \overline{\overline{S_{\rm tot}}}/\bar{\ell}$ and Curie constant density $c = \overline{\overline{S_{\rm tot}(S_{\rm tot}+1)}}/3\bar{\ell}$

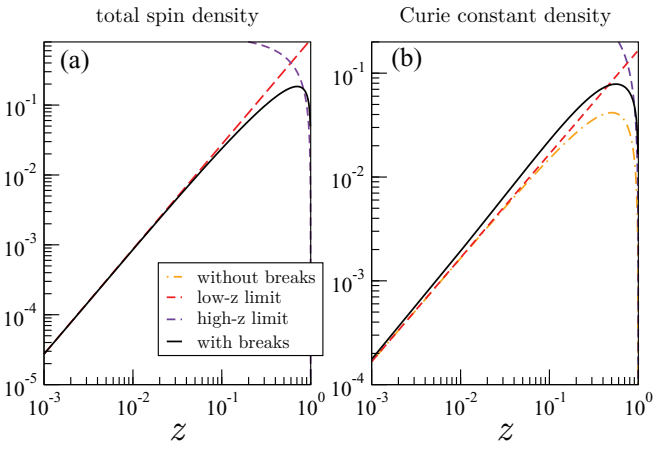

FIG. 10. (Color online) Effect of chain breaking on ladders. (a) Mean total spin density $\bar{\bar{s}}$ and (b) Curie constant density c averaged.

now read

$$\bar{\bar{s}} \simeq \tfrac{1}{2}\sqrt{z(1-z)\zeta} \tag{49}$$

and

$$c \simeq \frac{z}{6}(1-z)(1-\zeta) + \frac{1}{6}\sqrt{z(1-z)\zeta}, \tag{50}$$

which gives in the diluted limit, $z \ll 1$,

$$\bar{\bar{s}} \simeq \frac{\sqrt{3}}{2}z^{3/2} \quad \text{and} \quad c \simeq \frac{z}{6}(1+\sqrt{3z}+\cdots), \tag{51}$$

in agreement with the results of Sigrist and Furusaki[20] up to a prefactor.

In the opposite limit of high-density for impurities $z \to 1$, the system is equivalent to a few independent spin-1/2s, which essentially behave as in a paramagnetic phase. Therefore we have that $\bar{\bar{s}} \simeq 1-z$ and $c \simeq (1-z)/2$. In particular, we infer that there is an optimal doping z^o, which maximizes the Curie constant and a slightly different one that maximizes the total spin. The value of z^o is nontrivial since it occurs at the crossing of the two asymptotes.

These predictions are a lower bound for $\bar{\bar{s}}$ and c since very small clusters with a few sites have a total spin and susceptibility larger than the random-walk result. In order to show the quantitative role of chain breaking and the validity of the results, we plot on Fig. 10 the limiting behaviors at low- and high-doping z together with the formulas (49) and (50). Although these formulas are not exact, they capture well the existence of a maximum at an optimal doping.

IV. MODELS AND METHODS

A. Magnetization and Curie constant densities

We now turn to the effect of interactions on the magnetic curve of two-leg ladders doped with impurities. The magnetic excitation is denoted by H. We choose to define the total magnetization density as $m = \langle \hat{S}_z \rangle / L = 2\langle \hat{S}_z \rangle / N$ so that the high-field saturation density is $m_{\rm sat} = 1 - z$. With this normalization, the contribution of noninteracting impurities carrying a spin-1/2 to the magnetization is the Brillouin formula at temperature T (we set $k_B = 1$ in the following):

$$m(H,T) = z \tanh(H/2T), \tag{52}$$

where z thus corresponds to the *impurity* saturation magnetization, assuming that each impurity frees a spin-1/2. The latter assumption is actually affected by chain breaking and will be discussed in more details in Sec. VI.

In the low-field limit at finite-temperature, the Curie constant density c is defined as

$$c = T \left. \frac{\partial m}{\partial H} \right|_{H=0}. \tag{53}$$

In the case of independent impurities, we would have the total Curie constant $C_{z,N_i} = N_i/4$ corresponding to $c = C_{z,N_i}/(N/2) = z/2$, as expected from (52). If one uses the exact result (44) for correlated impurities, then the Curie constant density reads $c = z(1-z)/6$ without chain breaking or (50) with it.

B. Random dimer model

We first consider a simple model, dubbed "random dimer model" in which impurities are assumed to build dimers with their neighbor. Dimers are independent but have couplings randomly distributed according to $P(J)$. The magnetization of a single dimer of coupling J is given by

$$m_{\rm dimer}(H,T;J) = \frac{2\sinh(H/T)}{1 + e^{J/T} + 2\cosh(H/T)}. \tag{54}$$

The total number of dimers is $N_i/2$ so that the total magnetization density averaged over the coupling distribution reads

$$m(H,T) = 2z \int dJ\, P(J) \frac{\sinh(H/T)}{1 + e^{J/T} + 2\cosh(H/T)}. \tag{55}$$

The Brillouin formula (52) is recovered when $P(J) = \delta(J)$ or more physically, in the high-temperature limit when $T \gg J_{\rm max}$.

Taking the zero-field limit at finite temperature in (55) yields a temperature-dependent Curie constant $c(T)$:

$$c(T) = 2z \int dJ\, P(J) \frac{1}{3 + e^{\beta J}}, \tag{56}$$

which reaches the free spins result $c(T) = z/2$ in the high-temperature regime.

C. Solving the effective model

The effective Hamiltonian of interacting impurity spins is given by

$$\hat{\mathcal{H}}_{\rm imp} = \sum_{\mathbf{I},\mathbf{J}} J_{\rm eff}(\mathbf{I}-\mathbf{J}) \hat{\mathbf{S}}_\mathbf{I} \cdot \hat{\mathbf{S}}_\mathbf{J} \tag{57}$$

and is solved numerically using either ED for $N_i = 10$ or QMC up to $N_i = 100$ and provided there is no incommensurability,

i.e., for $q = \pi$. ED provides all energies $\{E_n(S_z)\}$ in a sector of total spin S_z so finite-temperature predictions are accessible. The couplings $J_{\rm eff}(\mathbf{I}-\mathbf{J})$ are obtained by sampling impurities configurations on a ladder and using either the approximate formula (22) with chosen q, J_0, and ξ, or the exact couplings computed from DMRG.

D. *Ab initio* calculations

Two "*ab initio*" methods are also used to compute observables directly on the original microscopic Hamiltonian (1): the DMRG technique, which gives accurate results for the zero-temperature magnetization curve, and QMC calculations well suited for finite-temperature dependence.

V. ZERO-FIELD SUSCEPTIBILITY AND THE TEMPERATURE-DEPENDENT CURIE CONSTANT

In this section, we focus on the limit of vanishing magnetic excitation $H \to 0$ at finite T. The order of limits matters and the situation $T \to 0$ for fixed H will be studied in the next section. In this limit, a modified Curie law is generically expected, written as

$$m(H,T) = \frac{c(T)}{T} H, \tag{58}$$

where $c(T)$ is a temperature-dependent Curie constant, corresponding to a static susceptibility $\chi(T) = c(T)/T$. The goal of this section is to investigate quantitatively the whole $c(T)$ curve and analyze the effect of interactions, doping, and frustration on its behavior. The various regimes of $c(T)$ in depleted ladders were first sketched by Sigrist and Furusaki[20] who gave the following picture: starting at high temperatures, the spins are essentially independent because of thermal fluctuations so that $c(T) \simeq (1-z)/2$. Assuming that the spin gap Δ_s is larger enough than the maximum coupling $J_{\rm max}$ (implicitly corresponding to the strong-coupling regime), lowering the temperature below the spin gap freezes all magnon excitations. Only spin-1/2s remain freed by impurities, which should behave independently for a range of temperatures $J_{\rm max} \lesssim T \lesssim \Delta_s$. This yields a plateau around $c \simeq z/2$ if one neglects chain breaking and $c \simeq z(1-z)/2$ if they are taken into account to first order corrections. Lowering again temperature enables one to reach the zero-temperature plateau discussed above and which is approximately given by $c \simeq z/6$ (the $z/12$ plateau within Ref. 20 conventions). In the regime governed by impurity-spins interactions, real-space renormalization group (RSRG) arguments[60] generally gives low-temperature corrections of the form

$$c(T) \simeq c(0) + K(T/J_{\rm max})^{\alpha}, \tag{59}$$

with K a nonuniversal constant and α an exponent that generally depends on doping z and that captures the interesting physics about impurities interactions. We now check and analyze this scenario using our various models and methods.

A. Hints from the random dimer model

The random dimer model formula (56) for the Curie constant already displays a nontrivial temperature dependence due to the coupling distribution. In the case of the power-law distribution (32) for which the exponent $\alpha = 2z\xi$ is the one of the couplings distribution and $J_{\rm max} = J_0$ [see below Eq. (60)], the high-temperature expansion leads to

$$c(T) = \frac{z}{2}\left[1 - \frac{1}{16}\frac{\alpha}{\alpha+2}\left(\frac{J_0}{T}\right)^2 + \frac{5}{768}\frac{\alpha}{\alpha+4}\left(\frac{J_0}{T}\right)^4 - \frac{77}{184\,320}\frac{\alpha}{\alpha+6}\left(\frac{J_0}{T}\right)^6 + \cdots\right],$$

while, at low T, a Sommerfeld-like expansion, in which the constant three appearing the denominator of (56) has to be carefully taken into account, yields a power-law:

$$\frac{c(T)}{2z} = \frac{1}{6} + K_\alpha \left(\frac{T}{J_0}\right)^{\alpha} \tag{60}$$

with the constant

$$K_\alpha = \frac{4}{9}\int_0^1 du(-\ln u)^\alpha \frac{1-u^2}{\left(1+\frac{10}{3}u+u^2\right)^2}. \tag{61}$$

K_α is of the order of 0.1–0.2 and matches some simple numbers for specific values of α: $K_0 = 1/12 \simeq 0.083\,333\ldots$, $K_1 = \frac{\ln 3}{6} \simeq 0.183\,102\ldots$. The curves for various α are represented in Fig. 11 and show that the prediction (60) works for a wide range of temperatures. In the limit of small α, one has the expansion $K_\alpha = 1/12 + K'\alpha$ with $K' = \frac{4}{9}\int_0^1 du \ln(-\ln u)\frac{1-u^2}{(1+\frac{10}{3}u+u^2)^2} \simeq 0.049\,366\,2\ldots$.

It is clear that, even though there is a power-law, there is nothing universal in this result. The scaling originates only from the fact that the distribution is a power law. Last, the zero-temperature result $c = z/3$, which already differs from free spins, is always expected in the case of a symmetric $J \to -J$ distribution.

B. Results on the effective model and a possible scenario for the low-temperature exponent

In *ab initio* ED and QMC calculations, the temperature-dependent Curie constant is computed exactly using the

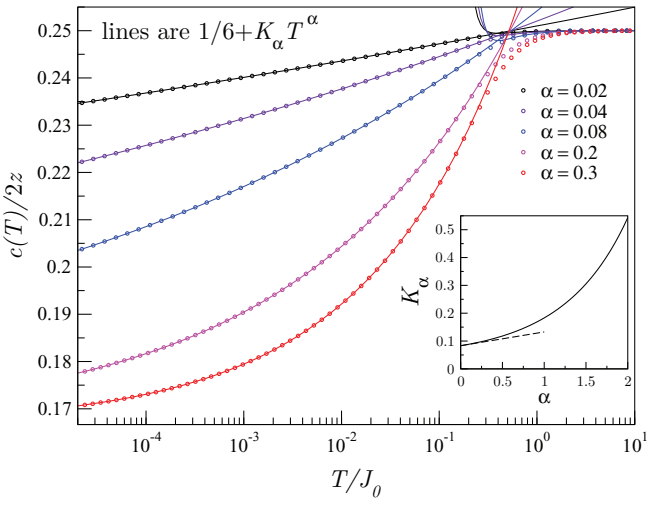

FIG. 11. (Color online) Curie constant within the random dimer model. In the ladder model, $\alpha = 2z\xi$. (Inset) Behavior of the constant K_α from (61).

average over thermal states and disorder configurations:

$$c(T) = \frac{2}{N} \frac{\overline{\sum_{S_z} \sum_n S_z^2 e^{-E_n(S_z)/T}}}{\sum_{S_z} \sum_n e^{-E_n(S_z)/T}}, \tag{62}$$

since $\langle S_z \rangle = 0$ when $H = 0$ for both the microscopic and effective models due to SU(2) symmetry. Notice that, on the effective model, chain breaking effects discussed in Sec. III C are not included.

1. ED results

We present on Fig. 12 the results obtained from exact diagonalization with $N_i = 10$ impurities and averaged over 10 000 samples. The first remarkable result is that the zero-temperature plateau is very well approximated on finite sizes by using (44) or its exact numerical evaluation. In fact, the effective model is not a bipartite lattice model to which the theorem applies, but the fact that it originates from a bipartite model to which the theorem applies (without frustration) seems to make it hold even in the effective model. The reason for that is certainly that the sign of the couplings satisfy the bipartite nature of the original lattice. The low-temperature departure from the $T = 0$ plateau is very sensitive to finite-size effects and disorder averaging. This makes it hard to capture the hypothetical thermodynamical behavior with this data. Yet, for the intermediate temperatures regime up to the high-temperature saturation plateau, we obtain a very good fit of the $c(T) - c(T = 0)$ data using a power-law, as one can see from Fig. 12(b). Collecting the fitted exponents Fig. 12(c) shows a very good agreement with the $2z\xi$ prediction of the random dimer model.

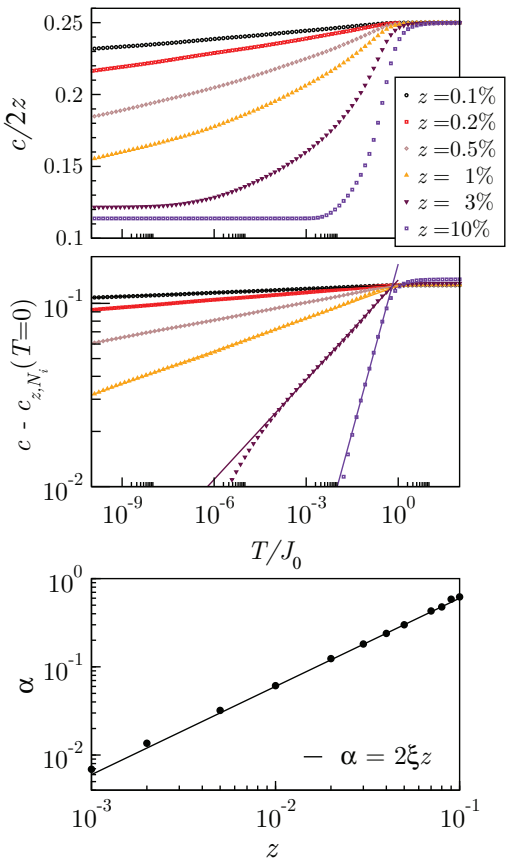

FIG. 12. (Color online) Exact diagonalization results on the thermal behavior of the Curie constant $c(T)$ within the effective model description for $N_i = 10$ impurities.

2. The RSRG scenario from the F-AF random chain

However, the behavior in the thermodynamical limit within the effective model is difficult to address. To sketch a possible scenario, we refer to the works done on the F-AF random chain.[58–61] Indeed, for reasonably short correlation lengths ξ, the effective model should fall into the F-AF universality class in the RSRG sense. This universality class has been dubbed as the large-spin phase, which is of the Griffith's type, and for which it has been found that the total spin follows the random-walk scenario discussed above, and that a power-law correction to the zero-temperature Curie constant is expected. As regards the possible universal exponents of this phase, it was found numerically[59] that it is strongly dependent on the singular nature of the initial coupling distribution. By denoting $P(J) \sim |J|^{-y}$ the initial distribution of the couplings, the following scenario is proposed: (i) when $y > y_c$ with $y_c \simeq 0.7$, the RSRG flows towards a nonuniversal fixed point with nonuniversal value of α. This exponent should depend on z and ξ but is not necessarily equal to $2z\xi$; (ii) when $y < y_c$ (initial distribution "not too singular"), the RSRG flows towards a universal fixed point with $\alpha \simeq 0.22$. QMC calculations[60,61] have demonstrated the following typical behavior for the Curie constant on the F-AF random chain; at high temperatures below the saturation plateau, $c(T)$ strongly depends on the initial distribution coupling. Yet, at low enough temperatures, the various $c(T)$ curves collapse very close to the RSRG prediction with $c(T) - c(0) = K(T/J_{\max})^{0.21}$, where $c(0) = 1/12$ and $K \simeq 0.117$.

Coming back to the situation of doped ladders, we may propose the following scenario. Provided the RSRG picture is applicable to the ladder, something certainly true for $z\xi \ll 1$ but hard to justify when $z\xi \sim 1$, we first expect from Refs. 60 and 61 that the high-temperature regime is always dependent on the distribution. Interestingly, in the doped ladder situation and within the random dimer picture, we found that this regime displays a power-law behavior with an exponent $2z\xi$, which is simply related to the coupling distribution exponent. Then, one expects that the RSRG picture develops at low-temperatures with two possible cases. The $y_c \simeq 0.7$ criteria translates on ladder to a critical doping $z_c \simeq 1 - e^{-0.15/\xi}$ such that (i) if $z < z_c$, the low-temperature exponent is nonuniversal, dependent on z and ξ and could differ from the high-temperature exponent expected to be $2z\xi$; (ii) if $z > z_c$, one can fall into the RSRG universality class and the low-temperature exponent should become independent of z and ξ and reaches 0.22. One must notice that the second situation can actually be realistic for doped ladders in the weakly coupled regime, since, for instance, $\xi \gtrsim 7$ for $J_\perp = J_\parallel/2$, giving $z_c \simeq 2\%$.

3. QMC results

In order to test this scenario, which relies on several questionable assumptions, although it looks plausible within

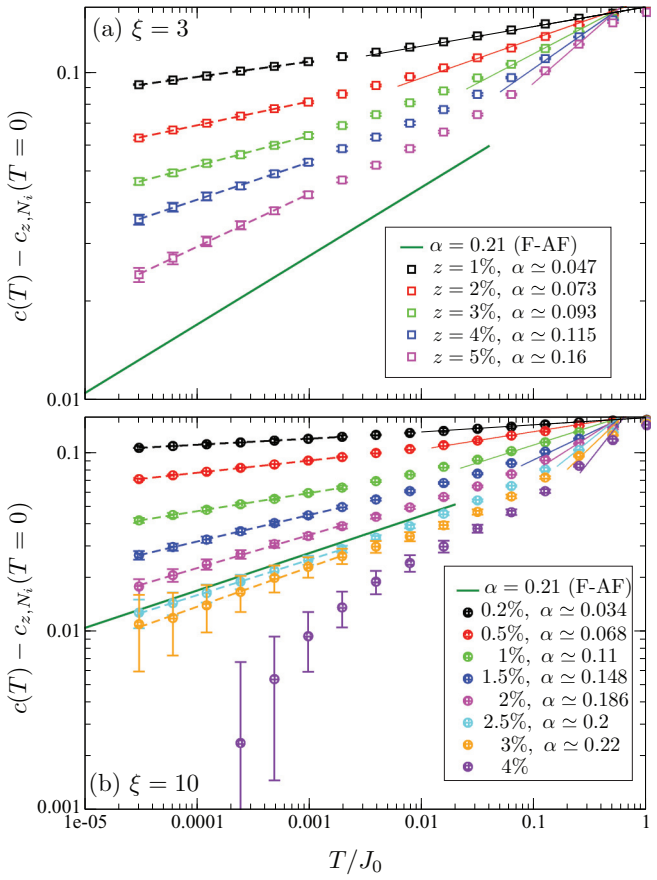

FIG. 13. (Color online) QMC results on the effective model with $N_i = 100$ impurities and two correlation length $\xi = 3$ (a) and 10 (b). Disorder averaging has been done over a few thousands of random configurations. The Curie constant per impurity (from which the asymptotic value $C_{z,N_i}/N_i$ has been subtracted) is shown vs temperature for various concentrations (symbols), together with power-law fits (dashed lines) of the form T^α, where $\alpha(z)$ is a varying exponent indicated on the plot. The lines in the high-temperature region are with exponent $2\xi z$. The $\alpha = 0.21$ line is the universal regime found in the F-AF chain by Frischmuth *et al.*,[60,61] including the same prefactor $K \simeq 0.117$.

the usual pictures discussed in random one-dimensional magnets, we have carried out QMC simulations on the effective model up to $N_i = 100$ impurities. The results for the Curie constant are plotted in Figs. 13(a) and 13(b) for two values of the correlation length $\xi = 3$ and 10, which respectively correspond to $z_c \simeq 0.048$ and $\simeq 0.015$. We observe on these data a crossover from a fast decaying high-temperature regime, roughly controlled by the exponent $2z\xi$ and a smaller doping-dependent exponent at lower temperatures. For large values of $z\xi$, the deviation is even clearer and the exponent does not seem to exceed the RSRG universal result of 0.21. We also show the F-AF universal result on the same plot showing that data at large ξz qualitatively saturates on this limit. These results give good confidence that the above scenario is plausible.

To further test the scenario, we have extracted the low-temperature exponent and plot it against z and ξz on Fig. 14. We observe that the low-doping regime is consistent with the $2\xi z$ limit, while intermediate dopings display significant deviations and a tendency to saturate around the RSRG universal regime for $z \gtrsim z_c$. Yet, the validity of the random F-AF RSRG picture can be questioned for two main reasons: when $z\xi$ becomes large, the dilute short range interaction limit fails and it is not guaranteed that the RSRG is still under control with longer range interaction. Second, as we will see on the magnetic curve, the discretized nature of the distribution can play a quantitative role. The criteria for the initial distribution exponent y is valid within a continuous description but the discretized nature of the coupling can make the distribution more singular. Interpretation in that sense was proposed on the same model through the study on correlation lengths.[33] Still, we observe that the RSRG argument does capture a lowering of the $\alpha(z)$ curve with respect to the $2\xi z$ naive expectation. Having an accurate quantitative description of this curve yet remains a challenging question.

4. *Effect of frustration and incommensurability*

Frustration makes the lattice nonbipartite so that the exact results (44) do not apply. Still, within the effective model, if frustration is not too strong, the system remains commensurate and the above results remain valid and shows that the behavior is the same. When frustration is large enough to induce incommensurability in the system, the effective model is affected and next-nearest neighbor couplings can become frustrating. In this situation, QMC calculations are not possible due to the sign problem and we carry out ED calculations limited to a $N_i = 10$ impurities. We do not show the data because the picture remains essentially and quantitatively the same as for the commensurate regime. This absence of strong qualitative differences is certainly due to the fact that the spin correlation length is small and prevents frustrating effects to develop on large scales. Furthermore, RSRG arguments tell that the commensurate and incommensurate cases should fall into the same F-AF random chain picture so that incommensurability does not actually plays a fundamental role in this model, at least on its one-dimensional version.

C. The full $c(T)$ curve from the microscopic model

We now discuss the overall behavior of $c(T)$ computed on the original microscopic model doped with impurities in order to test the scenario by Sigrist and Furusaki discussed above. We take the situation of an isotropic ladder which has $\xi \simeq 3$ but in which the energy scales J_0, $J_{\max}$ and J_1 are very close to each other (see Fig. 5). The first significant effect as seen on Fig. 15(a) is thus the absence of an intermediate plateau of independent impurity spins. Thermal magnons are activated before impurity spins become uncorrelated by thermal excitations so that the contributions of both can never be separated. This absence of plateau in the isotropic ladder will have its counterpart in the magnetic curve while scanning the energy scales with the magnetic field rather than with the thermal energy (see Sec. VI). In the large $J_\perp$ limit, the separation of energy scales suggests that the plateau could be visible but we have not checked it numerically.

At temperatures slightly below the temperature corresponding to the spin gap $T = \Delta_s$, a power-law behavior is clearly visible showing the regime in which the effective model

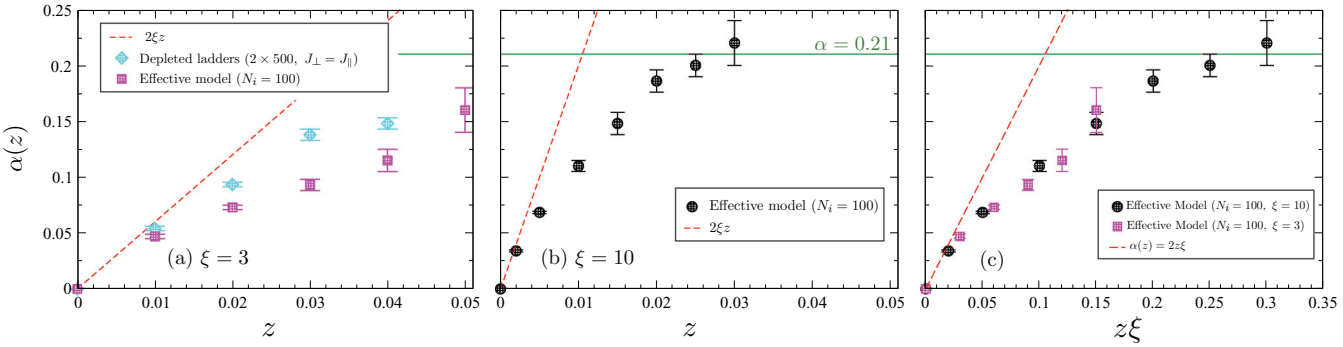

FIG. 14. (Color online) QMC estimates for the Curie constant exponent $\alpha(z)$ from the effective model with $N_i = 100$ impurities with (a) $\xi = 3$ and (b) $\xi = 10$. The horizontal $\alpha = 0.21$ lines indicate the RSRG universal regime of the F-AF chain. In (a), results for the depleted isotropic ladder are shown for comparison. The two cases $\xi = 3,10$ are also shown in (c) vs $z\xi$ where results seem to collapse on a single curve. In all cases, the exponent $\alpha(z)$ is smaller than the prediction $2z\xi$, which seems to hold only in the limit $z\xi \to 0$.

accounts for the physics. The exponent is found to depend on doping, with very small exponents at low dopings which could give the impression of the presence of a plateau, although this is not correct. A systematic extraction of the exponent [see Fig. 15(b)] gives the results plotted on Fig. 14 against the effective model results. Slightly larger exponents are found but the agreement can be viewed as correct considering the low values of the exponents and the difficulty to tackle this low-temperature regime numerically. Consequently, the effective model seems to capture the physics at low-energy of the interacting impurity spins. Although the convergence towards the universal RSRG regime is plausible at small $J_\perp$ and low doping from our results on the effective model, the numerical challenge it represents on the microscopic model is beyond the scope of this paper (the spin gap becomes significantly smaller).

VI. MAGNETIC CURVE AND DEVIATIONS FROM BRILLOUIN'S BEHAVIOR

Another way to probe the effective interactions between impurities is to scan the energies using a magnetic field rather than temperature. As we are studying the part of the magnetic curve that typically lies below the spin gap Δ_s, the results correspond to accessible magnetic fields, and are then particularly relevant to experimental measurements. We aim at proposing some possible relevant fits of this regime. Above the spin gap, the elementary excitations involve magnons that can localize in the disordered environment. There, the physics

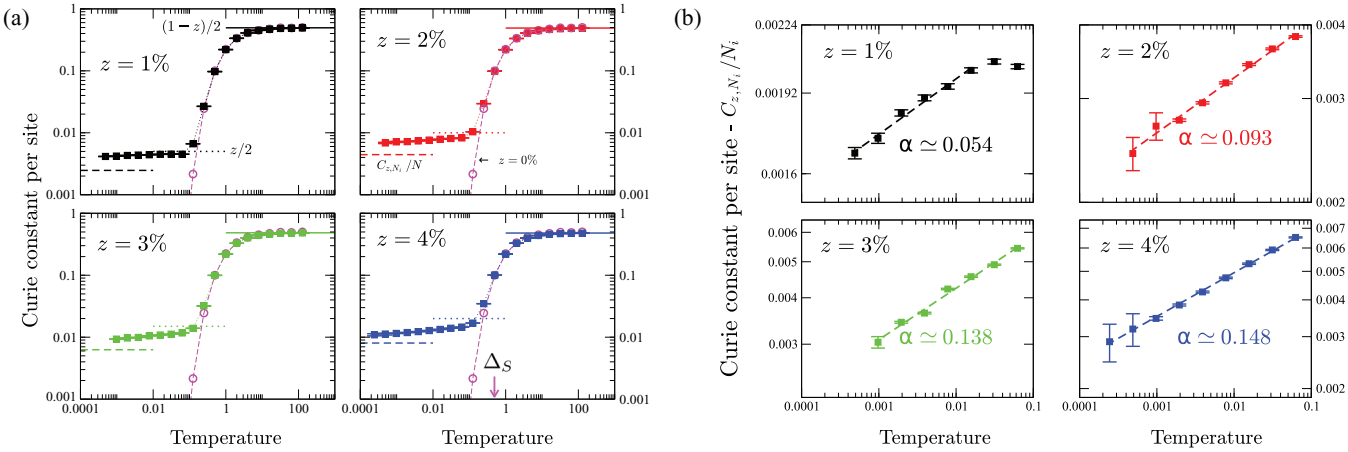

FIG. 15. (Color online) Finite temperature QMC results for the Curie constant per site of randomly depleted two-leg $S = 1/2$ isotropic ladders ($J_\perp = J_s = 1$) of total size $N = 2 \times 500$ sites with $N_i = 10,20,30,40$ nonmagnetic impurities, corresponding to $z = 1\%,2\%,3\%,4\%$, as indicated on the plots. QMC data have been averaged over several thousands of independent disordered samples. (a) The Curie constants are shown for the entire temperature regime. Full lines show the high-temperature free spin regime $c(T) = (1 - z)/4$; dotted lines the intermediate plateau regime at $z/4$ (roughly visible for $z = 1\%$ but absent for higher dopings); and dashed lines the expected very low-T limit $C_{z,N_i}/N_i$ computed in Sec. III A. The open magenta symbols show the Curie constant per site of the clean case, which start to deviate, rapidly falling to zero, below the spin gap Δ [arrow on the $z = 4\%$]. (b) Same data as in the left part from which the asymptotic Curie constant per site $C_{z,N_i}/N_i$ has been subtracted. One sees that the low-T part slowly goes to zero as power laws, with exponents $\alpha(z)$ indicated on the plot.

becomes quite different and we do not address these questions related to Bose-glass physics.

A. The zero-temperature magnetization jump and saturation plateau

We now turn to the generic behavior of the magnetic curve $m(H,T)$. In the previous section, the nontrivial behavior when $H \to 0$ at finite T was discussed. Physically, it corresponded to susceptibility measurements performed with $H \ll T$. Strictly speaking, we must have $m(H,T) = 0$ when $H = 0$ due to the SU(2) symmetry. If one now considers a finite system with $T = 0$ and a small but finite magnetic field, the degeneracy within a sector of total spin S will be lifted to favor the state $S^z = S$. Then, there exists a disorder averaged magnetization jump $\delta m = m(H = 0^+, T = 0) - m(H = 0, T = 0)$ that matches $\delta m = 2\overline{\langle S_z \rangle}/N = 2\overline{S}/N$. This is typical of a partially ferromagnetic state. If one does not take into account chain breaking effects, as we do for the effective model, the scaling of $\overline{S}$ yields a magnetization jump that vanishes in the thermodynamical limit as

$$\delta m \simeq \sqrt{\frac{2z(1-z)}{\pi}} \frac{1}{\sqrt{N}}. \tag{63}$$

Interestingly, we notice that, due to the random walk argument, the prefactor is actually related to the zero-temperature Curie constant c by $\delta m \sim \sqrt{c/N}$, which makes a connection between the two noncommutating limits of the magnetic responses under study. If we take chain breaking effects into account, then there exists a jump *even in the thermodynamical limit* which reads $\delta m = \overline{\overline{s}} \sim \frac{\sqrt{3}}{2} z^{3/2} \sim c^{3/2}$ in the diluted limit $z \ll 1$.

Lastly, one expects that, within a picture of impurities bringing each exactly one spin, the saturation plateau corresponding to the polarization of all these spins equals $m = z$. Yet, chain breaking effects should lower this value since configurations where two impurities are on the same rung do not bring any free spin. Taking this effect into account gives an expected saturation at $m = z(1-z)$. This effect matters for DMRG or QMC data as well as experiments.

B. Zero-temperature magnetic curves

1. Hints from the random dimer model

Using the random dimer model, the low-temperature magnetization curve (for $H \gg T$) takes a Fermi-Dirac form to a good approximation,

$$m(H,T) \simeq z \int dJ\, P(J) \frac{1}{e^{(J-H)/T} + 1}, \tag{64}$$

where H plays the role of the chemical potential. This is physically transparent as the system is equivalent in this limit to a collection of two-level systems with only the singlet and triplet $S_z = 1$ states contributing to the low-energy physics which naturally maps onto fermionic statistics.

In particular, the $T = 0$ limit of this model gives that the magnetic curve is simply related to the repartition function $R(J)$ of the couplings through $m(H,T=0) = zR(H)$. In the case of the continuous distribution (32), this yields a power-law behavior:

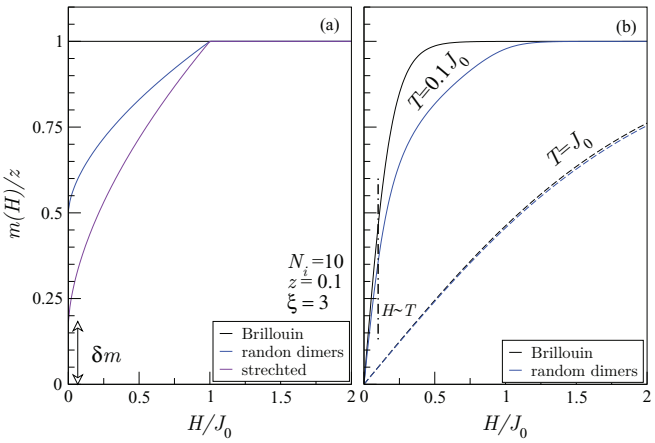

FIG. 16. (Color online) Schematic behavior of the magnetic curve from the random dimer picture at $T = 0$ (a) and finite temperature (b). δm represents the magnetization jump.

$$m(H,T=0) = \frac{z}{2}\left[1 + \left(\frac{H}{J_0}\right)^{\alpha}\right], \tag{65}$$

with $\alpha = 2z\xi$ and for $H \leqslant J_0$, which already deviates significantly from the Brillouin picture. It is important to notice that situation where $z > z^*$ from (35) is physical in the case of systems with a large correlation length $\xi \simeq 10$. Then, the curvature of the magnetic curve is expected to change from concave to convex.

Still, we see that the random dimer model fails to reproduce the correct $H \to 0$ limit and gives for the jump $\delta m = R(0)$ [$\delta m = 1/2$ for Eq. (65)]. One can incorporate the exact result (63) in the RDM by stretching the repartition function of antiferromagnetic couplings $R_+(J)$. We thus define the phenomenological "stretched random dimer" ansatz as

$$m(H,T=0) = \delta m + (z - \delta m) R_+(H). \tag{66}$$

Physically, the issue of the random dimer model is that it works with total spins $S = 0$ and $S = 1$ and cannot capture the large-spin formation. These features and ansatz of the random dimer model are represented on Fig. 16(a). Lastly, this rough understanding of the shape of the curve leads to the following simple power-law fit, which could be useful for experiments or numerical calculations:

$$m(H,T=0) = \delta m + (z - \delta m)\left(\frac{H}{J_0}\right)^{\alpha}, \tag{67}$$

in which one can leave free the three parameters δm, J_0, and α. Interestingly, RSRG arguments[59] have also proposed a power-law behavior for the magnetic curve when $H \gg T$ based on energy scales phenomenology.

2. Comparison between effective and microscopic models

We compute numerically the magnetization curves at zero temperature using DMRG on the microscopic model and average over many configurations. The results for the isotropic ladder $J_\perp = J_1$ are displayed on Figs. 17(a) and 17(b) for both a system without frustration and with frustration in the incommensurate regime. Qualitatively, the two curve are essentially governed by the coupling distribution and frustration does

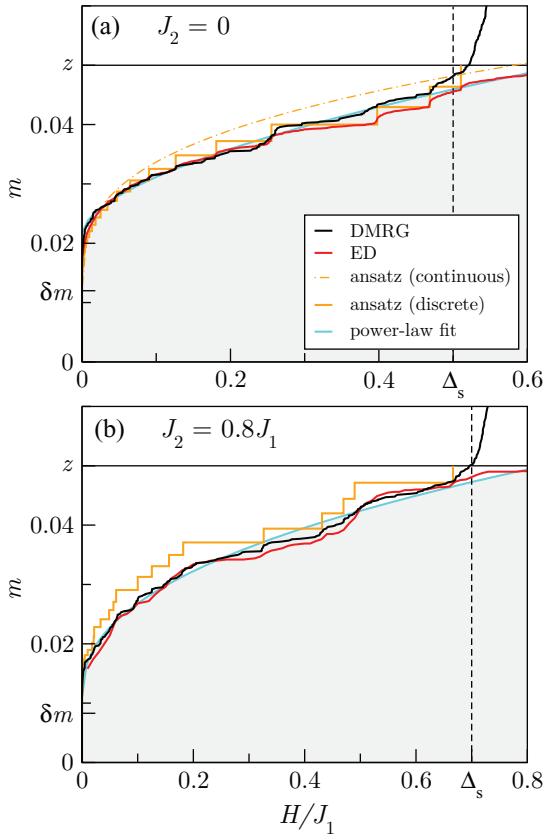

FIG. 17. (Color online) Comparison between DMRG on the microscopic model (isotropic ladder) and ED on the effective model: (a) in the commensurate regime and (b) in the incommensurate regime with frustration. The phenomenological "stretched" dimer model of (66) is also given using either the exact discrete or a continuous version of the couplings distribution. The power-law fit is done using (67) and provides a simple account of the deviation from the Brillouin response, which is emphasized by the grey area.

not have a drastic qualitative effect. Interestingly, the simple approximations described in the preceding section account rather well of the behavior of the curve. First, the ED on the effective model captures the power-law-like behavior and even underlines the discrete nature of the coupling distribution. This discrete nature is transparent from the ansatz (66) using the exact effective couplings. The DMRG does show faded steps corresponding to the larger couplings, and ED too. The envelope of the random dimer model is captured by the continuous version of the coupling distribution. Yet, we see that one really needs the discretized version to be quantitative. Last, we show that a fit of the form (67) captures the mean power-law behavior of the curve in a satisfactory way. This is all the more relevant as we will see that temperature tends to fade the steps due to the discrete couplings.

One can notice the slight difference between the ED and DMRG results. We attribute these to two main possible effects. First, as the systems are chosen to have the same total number of impurities, the limitation of the two-body interaction effective model can play a role. Many-impurity interactions could become relevant even though these are subdominant effects. Second, we have seen that chain breaking effects must make the saturation plateau occur at $z(1-z)$, but it also has the effect of averaging magnetic curves over various dopings. Indeed, in the presence of chain breaking effects, each piece has a different doping which approaches z on average but can be lower or higher. This should have significant effects compare to the fixed z curve of the ED on the effective model.

The last important remark is that no saturation plateau is reached in the isotropic ladder. As for the Curie constant plateau, this is due to the fact that the typical energy scales are of the same order of magnitude $J_0 \sim J_{\max} \sim \Delta_s$ (see Fig. 5). Then, magnons become activated by the magnetic field before all impurities are truly polarized. The energy scales separation in the strong-coupling limit suggests that such a plateau could be possible at large $J_\perp$ but we have not investigated this situation in details. In particular, the microscopic model displays small couplings in this limit which are harder to capture with DMRG.

C. Finite temperature

1. Random dimer model

The approximation of Eq. (64), naturally yields low-temperature corrections from a Sommerfeld expansion, valid provided $T \ll H$, which reads $m(H,T) = m(H,0) + \frac{\pi^2}{6} P'(H) T^2 + \cdots$, where $P'(H)$ is the derivative of the coupling distribution. For instance, in the case of the continuous distribution (32) and taking the approximation $z^* \simeq 1/(2\xi)$, the temperature corrections depend on doping and magnetic field through

$$m(H,T) = m(H,0) + \frac{\pi^2}{3} \frac{z(z-z^*)}{z^{*2}} \left(\frac{H}{J_0}\right)^{\frac{z}{z^*}} \left(\frac{T}{H}\right)^2 .$$

Here again, the response to a small temperature is expected to strongly depend on the side of the limiting case $z = z^*$, displaying a change in sign on the corrections. In the particular situation where $z = z^*$, for which $P(J)$ is flat, the magnetization curve of the random dimer model can actually be computed exactly:

$$m(H,T) = z \frac{\sinh(H/T)}{1+2\cosh(H/T)} \times \frac{T}{J_0} \ln\left\{ \frac{1+e^{J_0/T}[1+2\cosh(H/T)]}{1+e^{-J_0/T}[1+2\cosh(H/T)]} \right\}.$$

Following the previous remark on the inability of the random dimer model to account for the large-spin formation, we can devise an extension of the stretched dimer model at finite temperatures using the following ansatz:

$$m(H,T) \simeq \delta m \tanh\left(\frac{H}{2T}\right) + \frac{z-\delta m}{1-R(0)} \int_{J>0} m_{\text{dimer}}(H,T;J) p(J) dJ, \quad (68)$$

where the first part accounts for the contribution of ferromagnetic couplings, while the second accounts for the magnetization process of antiferromagnetic dimers. The first term should in principle correspond to a Brillouin function of spin $\bar{S}$ but this version already gives satisfactory results.

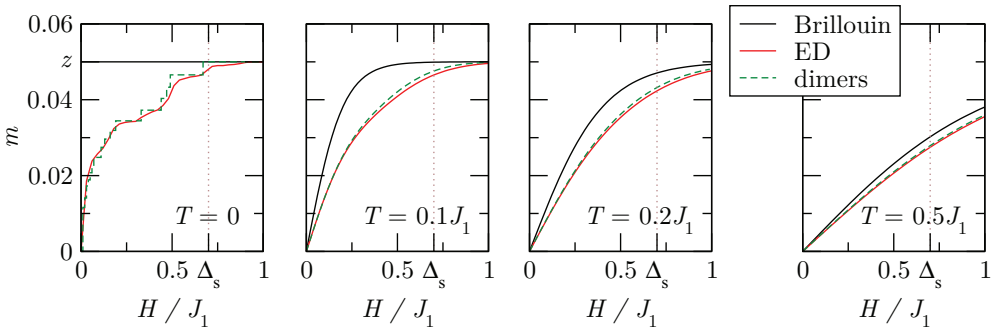

FIG. 18. (Color online) Comparison between the Brillouin result for independent spin, the ED curve on the effective model and the phenomenological "stretched" random dimer model at finite temperature from Eq. (68). Four increasing temperatures are given.

2. *Comparison with ED and QMC*

The effect of temperature is first discussed on Fig. 18 by showing the comparison between the Brillouin response to the ED and random dimer model predictions for four increasing temperatures. All curves should collapse at high temperatures $T \gg J_{\max}$. We see that the zero-temperature steps are rapidly faded as temperature is turn on. Still, the deviation from the Brillouin curve due to the interaction remains well visible for finite temperature and actually makes the random dimer model almost exact.

In order to validate the above comparison, we have compared the ED on the effective model to QMC, which is the appropriate method for finite temperature calculations on the microscopic model. In Fig. 19, one observes a rather good agreement for several realistic dopings. The larger the doping, the larger the deviation from the Brillouin curve is and the larger the distance from saturation is when the magnons set in. The slight difference between ED and QMC could here again be attributed to many-impurity interactions not taken into account in the effective model and also to the effective doping averaging induced by chain breaking effects, as for the zero-temperature curve. Then, the following message is almost quantitatively correct from the comparison between all different approaches: the low-part of the magnetic curve probes the couplings distribution between the impurities. This is evident in the random dimer model and the picture survives to the microscopic model rather well. This simple analysis is certainly due to the fact that we are discussing a simple observable (density of magnetization), which is little affected by low-energy behavior or correlations in the system. Therefore it could be accessible and interesting to test such phenomenology in experiments working with quasi-one-dimensional systems.

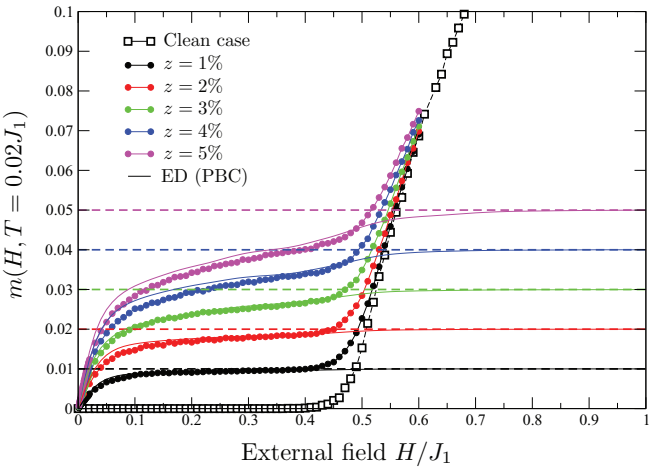

FIG. 19. (Color online) QMC results for the longitudinal magnetization vs external field H/J_1 of depleted ladders of size $N = 2 \times 500$ sites, averaged over ∼500 disordered samples, at finite temperature $T/J_1 = 0.02$. Different impurity concentrations $z =$ 1%,2%,3%,4%,5% are shown, together with the clean case at the same temperature for comparison. Horizontal dashed lines show the expected saturation value for the impurities $m_{\text{sat}} = z$, and the full lines are ED results obtained with PBC on 1000 random clusters of 10 impurities from which one clearly sees that the saturation value is only reached when $H/J_1 \to 1$.

D. Consequences for experiments

Our theoretical study could in principle apply to several realistic spin gapped materials. However, as seen above, a clear separation between different energy scales—the spin gap Δ_s below which free local moments are expected, and the largest effective coupling $J_{\max}$ below which they start to correlate upon random F-AF exchanges—would be difficult to achieve in systems close to the isotropic ladder limit. The separation remains plausible in the strong-coupling limit, although we have not investigate this point quantitatively in this paper. In the isotropic case, a saturation regime of impurity spins will be hardly detectable. Nevertheless, the regime of large spin could be detected in Curie tails at low temperature, provided the three dimensional ordering of induced moments (expected below temperatures set by three dimensional couplings) occurs at low enough temperature. In such a respect, a new analysis of susceptibility data of Zn ($S = 0$) or Ni ($S = 1$) doped $BiCu_2PO_6$ form Ref. 16 may give interesting results, although the three dimensional ordering of induced moments occurs below a few degrees of Kelvin.[46] Perhaps more promising is the doped Haldane chain system Y_2BaNiO_5[34,35,91] where a very small interchain coupling $\sim 10^{-1}$ K is expected from neutron scattering[92] despite a very large spin gap $\Delta_s \simeq 100$ K.

More generally, our study clearly shows that Curie tails, present in all AF materials even for undoped ones, because of intrinsic defects or Imry-Ma domain formation with random couplings,[93] have to be analyzed perhaps more carefully than

what is usually done. In particular, the assumption of free impurities leading to the extraction of their concentration z through the simple form $\chi_{\rm imp} = z/(4T)$ is not expected to be valid in many experimental situations.

Regarding the magnetization curve, our work can potentially apply to many materials where Brillouin-like responses are observed upon increasing the external field. For spin-gapped systems, the effective couplings between local moments can strongly renormalize downwards the Brillouin-like magnetization and pushes the saturation towards larger magnetic fields, possibly larger than the spin gap Δ_s. This means that, at the critical field where magnon excitations start to appear, not all impurity-induced moments have been saturated. Such a phenomenology is expected for $BiCu_2PO_6$ in a field.[51,94] Nevertheless, for this ladder material,[51] and also for other systems such as the Herbertsmithite Kagomé compound,[95] the presence of non-negligible Dzyaloshinskii-Moriya (DM) anisotropies make the situation much more difficult to analyze since DM terms induce a finite magnetic response also below the spin gap. The modification of the Brillouin-like response due to the competition between impurity physics and DM interactions in an external field at finite temperature is a very interesting subject, relevant for many realistic systems, that we leave for future studies.

VII. CONCLUSION

The physics of randomly depleted ladder, studied initially in the seminal work of Sigrist and Furusaki,[20] offers a remarkable playground for studying the effect of impurity disorder in gapped systems without and with frustration. In this contribution to the field, we improved on several intuitive results of Ref. 20 to provide quantitative predictions and comparison to numerics and adressed the shape of the magnetization curve. Based on a detailed analysis of the effective couplings between impurities and of the corresponding coupling distribution, we focused the main two magnetic responses: the zero-field susceptibility, through the temperature-dependent Curie constant, and the magnetization curve. The first one is shown to have a nontrivial power-law behavior at very-low temperature in qualitative agreement with a RSRG scenario. The high-temperature deviation from free impurity spins is well captured by a simple random dimer model. This model also accounts qualitatively well for the magnetization curve for which we give several phenomenological fits at zero and finite temperature, which are in good agreement with accurate numerical calculations. One of the key outcome of this study is that incommensurability (induced by frustration) plays little role in the local quantities we looked at. Indeed, the main consequence of incommensurability is a mere reduction of the zero-temperature spontaneous magnetization and of the low-temperature limit of the Curie constant. The situation might be different in higher dimensional system but the one-dimensional version seems to be in the same universality class, as expected from RSRG arguments. These predictions on the magnetic responses could motivate experiments in that direction since the required temperatures and magnetic fields are accessible for several compounds.

ACKNOWLEDGMENTS

A.L. thanks Cécile Delaporte and Antoine Channarond for insightful discussions on Markov chains calculations. A.L. and G.R. acknowledge support from the French ANR Program ANR-2011-BS04-012-01 QuDec. N.L. acknowledge GENCI (Grants No. 2012-x2012050225 and No. 2013-x2013050225) and CALMIP for numerical resources and the French ANR Program ANR-11-IS04-005-01.

APPENDIX A: CORRELATIONS AND SUSCEPTIBILITY IN THE BOND-ORDER MEAN-FIELD APPROXIMATION

In this appendix, we detail the calculation of the spin correlation functions within the bond-order mean-field theory developed for the frustrated ladder in Ref. 53. We will use the same notations as in this reference. The dynamical and static structure factors of the model has also been addressed recently in Ref. 54.

1. Notations and useful relations from BOMF

Within BOMF theory in which the singlet operators on rungs are assumed to condense $\langle s_i \rangle = \bar{s}$, the mean-field Hamiltonian is solved through a Bogoliubov transformation on the triplet operators in k-space $t_{k,\sigma}$

$$b_{k\sigma} = u_k t_{k\sigma} + v_k t^\dagger_{-k\sigma}, \tag{A1}$$

where u_k and v_k satisfy $u_k^2 - v_k^2 = 1$. This leads to the diagonal version of the Hamiltonian

$$\mathcal{H}_m = E_0 + \sum_k \omega_k b^\dagger_{k\sigma} b_{k\sigma}, \tag{A2}$$

where ω_k is the dispersion relation that depends on $\bar{s}$ and the chemical potential μ used to enforce the hard-core nature of the triplets on rungs. These two parameters are usually computed self-consistently with numerical methods.

In this paper, in order to have tractable analytical formulas, we use the following approximations, which turn out to be good in the strong-coupling limit, $\bar{s} \simeq 1$ and

$$\omega_k \simeq J_\perp \sqrt{1 + \frac{J_1}{J_\perp}\cos k + \frac{J_2}{J_\perp}\cos 2k}. \tag{A3}$$

The zeros of ω_k extended to the complex plane will control the singularities of most physical quantities. To this end, we introduce the polynomial

$$P(X) = 2\frac{J_2}{J_\perp}X^2 + \frac{J_1}{J_\perp}X + 1 - \frac{J_2}{J_\perp}, \tag{A4}$$

such that

$$\omega_k \simeq J_\perp \sqrt{P(\cos k)}. \tag{A5}$$

2. Spin structure factor and real-space correlations

In Ref. 53, we obtained that the spin structure factor defined by

$$S_k = \sum_{x=1}^{L} e^{ikx} \mathcal{S}_x, \tag{A6}$$

where $\mathcal{S}_x = \langle (\mathbf{S}_{x,1} - \mathbf{S}_{x,2}) \cdot (\mathbf{S}_{1,1} - \mathbf{S}_{1,2}) \rangle$ are real-space spin correlations, is given in the BOMF approximation by

$$S_k = \frac{3\bar{s}^2}{\sqrt{P(\cos k)}}. \tag{A7}$$

We now give more details on the two commensurable and incommensurable regimes, limited to the strong-coupling regime. We recall that the transition occurs at $J_{2,c} \simeq J_1/4$. (i) For $J_2 < J_{2,c}$, P has two real roots, lower than -1. Consequently, S_k has branch cuts and four branching points on the axis $\Re[k] = \pi$, with imaginary parts denoted by $\pm 1/\xi^{\pm}_{\rm spin}$ that define two correlation lengths $\xi^{\pm}_{\rm spin}$ ($\xi^{+}_{\rm spin} > \xi^{-}_{\rm spin}$), such that

$$\xi^{\pm}_{\rm spin} \simeq \text{arcosh}^{-1} \left(\frac{J_1 \mp \sqrt{J_1^2 - 4J_2 J_\perp}}{4J_2} \right), \tag{A8}$$

in the strong-coupling limit. (ii) For $J_2 = J_{2,c}$, P factorizes exactly and the square root disappears in the denominator of S_k. There is no longer branch cuts and the branching points merge to give two poles on the axis $\Re[k] = \pi$, with imaginary part $\pm 1/\xi_{\rm spin}$, where

$$\xi_{\rm spin} = \text{arcosh}^{-1} \left(\frac{J_1}{4J_2} \right), \tag{A9}$$

(iii) For $J_2 > J_{2,c}$, the roots of P have a nonzero imaginary part. Consequently, the branching points leaves the axis $\Re[k] = \pi$. There coordinates can be written as $\pm q \pm i\xi^{-1}_{\rm spin}$, where q is the incommensurate wave-vector associated to the real-space correlations and $\xi_{\rm spin}$ is the spin correlation length. In the large $J_\perp$ limit, we obtain

$$q \simeq \arccos \left(-\frac{J_1}{2\sqrt{J_2 J_\perp}} \right), \tag{A10}$$

$$\xi_{\rm spin} \simeq \text{arcosh}^{-1} \left(\frac{1}{2} \sqrt{\frac{J_\perp}{J_2}} \right). \tag{A11}$$

Real-space behavior of the correlation function is recovered after a Fourier transform of the static structure factor:

$$\mathcal{S}_x = \frac{3\bar{s}^2}{2\pi} \int_0^{2\pi} \frac{e^{ikx}}{\sqrt{P(\cos k)}} dk. \tag{A12}$$

One cannot easily compute this integral using the theorem of residues, because of the branch cuts, but one can argue that the behavior in x is essentially controlled by $e^{iz_1 x}$ et $e^{iz_2 x}$ with z_1 and z_2 the singularities of S_k in the upper half plane. Furthermore, due to the presence of the square root in the denominator, one may guess the following asymptotic behavior

$$\int_0^{+\infty} \frac{e^{ikx}}{\sqrt{k^2 + \xi^{-2}}} dk \underset{x \gg \xi}{\sim} \frac{e^{-x/\xi}}{\sqrt{x}}. \tag{A13}$$

Indeed, as for the J_1-J_2 chain,[96] the $1/\sqrt{x}$ correction yields better fits of the numerical results. We thus have the following scenario for the correlation functions. (i) For $J_2 < J_{2,c}$, in the commensurate regime:

$$\mathcal{S}_x \sim \frac{(-1)^x}{\sqrt{x}} (A e^{-x/\xi^{+}_{\rm spin}} - B e^{-x/\xi^{-}_{\rm spin}}), \tag{A14}$$

where $\xi^{\pm}_{\rm spin}$ are given by (A8) and A and B are two constants that depend on $\xi^{\pm}_{\rm spin}$. (ii) For the transition point $J_2 = J_{2,c}$, we remark that the factorization of the denominator makes the decay purely exponential. Then, one expects

$$\mathcal{S}_x \sim C(-1)^x e^{-x/\xi_{\rm spin}}, \tag{A15}$$

with $\xi_{\rm spin}$ given by (A9) and C a constant depending on$\xi_{\rm spin}$.

(iii) For $J_2 > J_{2,c}$, in the incommensurate regime:

$$\mathcal{S}_x \sim C' \frac{e^{-x/\xi_{\rm spin}}}{\sqrt{x}} \cos(qx + \phi), \tag{A16}$$

where q and $\xi_{\rm spin}$ are given by (A10) and (A11), and C' and ϕ are constant depending on q and $\xi_{\rm spin}$.

3. Susceptibility

In order to compute the magnetic susceptibility at $\mathbf{k} = (k,\pi)$, one applies a magnetic field corresponding to the wave vector $\mathbf{k}$

$$\mathbf{H_r} = H \cos(\mathbf{k} \cdot \mathbf{r})\, \mathbf{e}_z. \tag{A17}$$

In the BOMF approximation, the Hamiltonian then reads

$$\mathcal{H} = E_0 + \sum_{k',\sigma} \omega_{k'} b^\dagger_{k'\sigma} b_{k'\sigma} - \frac{L}{2} H\bar{s}(u_k - v_k)(b_{k0} + b_{-k0} + b^\dagger_{k0} + b^\dagger_{-k0}). \tag{A18}$$

The energy correction is obtained from second order perturbation theory in H as

$$E \simeq E_0 - L\bar{s}^2 \frac{(u_k - v_k)^2}{2\omega_k} H^2, \tag{A19}$$

By definition, the susceptibility $\chi_{\mathbf{k}}$ enters in the expression through linear response theory

$$E \simeq E_0 - L(\chi_{\mathbf{k}} + \chi_{\mathbf{-k}}) H^2 \tag{A20}$$

from which we deduce the following expression for the static susceptibility:

$$\chi_{k,\pi} = \frac{\bar{s}^2}{J_\perp - 4\mu} \frac{1}{P(\cos k)}, \tag{A21}$$

where P is the polynom defined in (A4).

a. Magnetization profile

Using the result for the susceptibility, on gets for the magnetization profile the prediction

$$\langle S^z_{x,y} \rangle \simeq \frac{1}{8}(-1)^y \frac{1}{2\pi} \int_0^{2\pi} \frac{e^{ikx}}{P(\cos k)} dk, \tag{A22}$$

where the position (x,y) are relative to the impurity site. The integral can be computed with help of the residues theorem

applied over a rectangle of base between 0 and 2π and infinite in the vertical direction.

APPENDIX B: COUPLINGS DISTRIBUTION IN THE INCOMMENSURATE CASE

Performing the change of variables requires the calculation of the derivative

$$\frac{dJ}{dr} = -\frac{J(r)}{\xi}[1 + q\xi \tan(qr+\phi)] \tag{B1}$$

$$= -\frac{J(r)}{\xi}\left[1 + q\xi\sqrt{\left(\frac{J_0}{J(r)}\right)^2 e^{-2r/\xi} - 1}\right]. \tag{B2}$$

The zeros of the derivative of denoted by r_m and satisfy the equation

$$\tan(qr_m + \phi) = -\frac{1}{q\xi} = -\tan\theta \tag{B3}$$

with $\theta = \arctan\left(\frac{1}{q\xi}\right) \in [0,\pi/2]$. Consequently, we have the zeros

$$r_m = (m\pi - \theta - \phi)/q > 0 \quad \text{with} \quad m = 1,2,3,\ldots \tag{B4}$$

One can take by convention $r_0 = 0$ to define the intervals in which the sign of the derivative is constant $I_m = [r_m, r_{m+1}]$. It is clear that the intervals have the same size $r_{m+1} - r_m = \pi/q$. Formally, one can write

$$\delta(J - J(r)) = \sum_{r_k^*|J(r_k^*)=J} \left|\frac{dJ}{dr}\right|^{-1}_{r=r_k^*} \delta(r - r_k^*).$$

The solutions $r_k^*(J)$ of the equation $J(r) = J$ are not analytically computable in general. For a given J, there is at most one solution in each interval I_m and there is a least one solution for $|J| \leqslant J_0$. Let us denote by $S(J)$ the number of solutions at a given J so that the index ranges $1 \leqslant k \leqslant S(J)$. Using (B2), we have

$$\delta(J - J(r)) = \sum_{k=1}^{S(J)} \frac{\xi}{|J| + q\xi\sqrt{J_0^2 e^{-2r_k^*(J)/\xi} - J^2}} \delta(r - r_k^*(J)).$$

We restrict the discussion to the continuous distribution case since the analytical formula for the discrete version do not help with respect to a direct numerical sampling. In this case, the weighting by the continuous approximation for $p(\mathbf{r})$ gives

$$P(J) = z\xi \sum_{k=1}^{S(J)} \frac{e^{-2zr_k^*(J)}}{|J| + q\xi\sqrt{J_0^2 e^{-2r_k^*(J)/\xi} - J^2}}.$$

The reduction of probability of large J is understood by studying the situation where $J \lesssim J_0$ so that there is only a single solution $r_1^*(J)$. Then, one can write

$$r_1^*(J) = \xi \ln\left(\frac{J_0}{|J|}\right) - \delta r \tag{B5}$$

with $\delta r > 0$ since the effect of q is to decrease the position of the solution with respect to the $q = \pi$ result. This gives

$$P(J) = P_{q=\pi}(J)\frac{e^{2z\delta r(J)}}{1 + q\xi\sqrt{e^{2\delta r(J)/\xi} - 1}}.$$

Although it is not obvious in the formula, one may convince one-self graphically that $P(J) < P_{q=\pi}(J)$ corresponding to a decrease of the weight at large J. Consequently, the weight of small Js increase since the signal can approach zero at any distance.

APPENDIX C: DISTRIBUTION OF LADDER SIZES

In this appendix, we study the distribution of sizes of disconnected ladders $\rho(\ell)$ for a given impurity doping z. If we consider an impurity at position $(x,0)$, there are three positions for a second impurity that break the ladder: $(x-1,1)$, $(x,1)$ and $(x+1,1)$. In the diluted limit $z \ll 1$, the density of cuts is then $3z^2$ and the average length of disconnected ladders $\bar{\ell} \simeq 1/3z^2$. As the cuts are not correlated (at least at large enough distances), it is reasonable to assume that the number of cuts follows a geometric law of parameter $\zeta \simeq 3z^2$:

$$\rho(\ell) \simeq \zeta(1-\zeta)^\ell. \tag{C1}$$

In fact, the distribution can be calculated exactly. For this, the ladder is described by a Markov chain $(X_n)_{n\geqslant 0}$, where X_n represents the configuration of the plaquette made of the two consecutive rungs n and $n+1$ (see Fig. 20). The Markov property is verified: the configuration on plaquette $n+1$ only depends of the configuration on plaquette n as they have a rung in common. The 2^4 configurations on a plaquette are classified as follows: (1) the plaquette dos not break the ladder and there is no impurity on the second rung, (2) the plaquette dos not break the ladder and there is one impurity on the second rung, and (3) the plaquette breaks the ladder.

The transition matrix Q, whose elements are the probabilities to go to configuration j from configuration i, writes

$$Q = \left(\begin{array}{cc|c} & & z^2 \\ \multicolumn{2}{c|}{\raisebox{1.5ex}{$\widetilde{Q}$}} & z \\ \hline 0 & 0 & 1 \end{array}\right), \tag{C2}$$

where

$$\widetilde{Q} = \begin{pmatrix} (1-z)^2 & 2z(1-z) \\ (1-z)^2 & z(1-z) \end{pmatrix}. \tag{C3}$$

The transition probabilities from configuration 3 are not needed and we can take this configuration as a trap state. We want to calculate the distribution of distances to reach

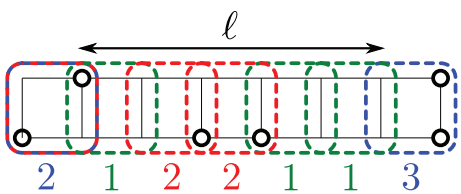

FIG. 20. (Color online) Schematics of the Markov chain process for chain breaks in the ladder.

configuration 3

$$\rho(\ell) = \mathbb{P}(X_{\ell+1} = 3, X_\ell \neq 3, \ldots, X_0 \neq 3), \tag{C4}$$

starting from an initial distribution for X_0

$$P_0 = (p1 - p0). \tag{C5}$$

Equation (C4) can be expanded as

$$\rho(\ell) = \zeta_\ell \prod_{n=0}^{\ell-1} (1 - \zeta_n), \tag{C6}$$

where

$$\begin{aligned} \zeta_n &= \mathbb{P}(X_{n+1} = 3 | X_n \neq 3) \\ &= \frac{z^2 \mathbb{P}(X_n = 1) + z\mathbb{P}(X_n = 2)}{\mathbb{P}(X_n = 1) + \mathbb{P}(X_n = 2)} . \end{aligned} \tag{C7}$$

One can easily show by mathematical induction that

$$\mathbb{P}(X_n = i) = (P_0 Q^n)_i . \tag{C8}$$

As a result, we have

$$\zeta_n = \frac{(p1 - p)\widetilde{Q}^n \binom{z^2}{z}}{(p1 - p)\widetilde{Q}^n \binom{1}{1}} . \tag{C9}$$

The distribution (C6) is not exactly a geometric law but ζ_n converges really quickly to a constant

$$\zeta = \tfrac{1}{2}[1 + z - (1 - z)\sqrt{1 + 4z(1 - z)}], \tag{C10}$$

independent of p, that is, independent of the initial distribution P_0. In the limit $z \ll 1$, one recovers $\zeta \simeq 3z^2$.

The mean cluster size thus has the following low-z expansion

$$\bar{\ell} = \frac{1}{3z^2}\left(1 + 2z - \frac{4}{3}z^2 + 4z^3 + \cdots\right). \tag{C11}$$

On the other limit $z \to 1$, $\bar{\ell} \to 1$, as expected.

*arthur.lavarelo@u-psud.fr
†guillaume.roux@u-psud.fr
‡nicolas.laflorencie@irsamc.ups-tlse.fr

[1] H. Alloul, J. Bobroff, M. Gabay, and P. J. Hirschfeld, Rev. Mod. Phys. **81**, 45 (2009).
[2] A. C. Hewson, *The Kondo Problem to Heavy Fermions* (Cambridge University Press, Cambridge, UK, 1997), Vol. 2.
[3] F. Evers and A. D. Mirlin, Rev. Mod. Phys. **80**, 1355 (2008).
[4] M. P. A. Fisher, P. B. Weichman, G. Grinstein, and D. S. Fisher, Phys. Rev. B **40**, 546 (1989).
[5] K. Sato, L. Bergqvist, J. Kudrnovský, P. H. Dederichs, O. Eriksson, I. Turek, B. Sanyal, G. Bouzerar, H. Katayama-Yoshida, V. A. Dinh, T. Fukushima, H. Kizaki, and R. Zeller, Rev. Mod. Phys. **82**, 1633 (2010).
[6] K. Binder and A. P. Young, Rev. Mod. Phys. **58**, 801 (1986).
[7] E. Dagotto and T. M. Rice, Science **271**, 618 (1996).
[8] D. C. Johnston, J. W. Johnson, D. P. Goshorn, and A. J. Jacobson, Phys. Rev. B **35**, 219 (1987).
[9] T. Barnes, E. Dagotto, J. Riera, and E. S. Swanson, Phys. Rev. B **47**, 3196 (1993).
[10] S. Gopalan, T. M. Rice, and M. Sigrist, Phys. Rev. B **49**, 8901 (1994); B. Normand and Ch. Rüegg, *ibid.* **83**, 054415 (2011).
[11] M. Azuma, Z. Hiroi, M. Takano, K. Ishida, and Y. Kitaoka, Phys. Rev. Lett. **73**, 3463 (1994).
[12] M. Azuma, Y. Fujishiro, M. Takano, M. Nohara, and H. Takagi, Phys. Rev. B **55**, R8658 (1997).
[13] M. Azuma, M. Takano, and R. S. Eccleston, J. Phys. Soc. Jpn. **67**, 740 (1998).
[14] N. Fujiwara, H. Yasuoka, Y. Fujishiro, M. Azuma, and M. Takano, Phys. Rev. Lett. **80**, 604 (1998).
[15] S. Ohsugi, Y. Tokunaga, K. Ishida, Y. Kitaoka, M. Azuma, Y. Fujishiro, and M. Takano, Phys. Rev. B **60**, 4181 (1999).
[16] B. Koteswararao, A. V. Mahajan, L. K. Alexander, and J. Bobroff, J. Phys.: Condens. Matter **22**, 035601 (2010).
[17] F. Casola, T. Shiroka, S. Wang, K. Conder, E. Pomjakushina, J. Mesot, and H.-R. Ott, Phys. Rev. Lett. **105**, 067203 (2010).
[18] S. R. White, R. M. Noack, and D. J. Scalapino, Phys. Rev. Lett. **73**, 886 (1994).
[19] H. Fukuyama, N. Nagaosa, M. Saito, and T. Tanimoto, J. Phys. Soc. Jpn. **65**, 2377 (1996).
[20] M. Sigrist and A. Furusaki, J. Phys. Soc. Jpn. **65**, 2385 (1996).
[21] N. Nagaosa, A. Furusaki, M. Sigrist, and H. Fukuyama, J. Phys. Soc. Jpn. **65**, 3724 (1996).
[22] Y. Motome, N. Katoh, N. Furukawa, and M. Imada, J. Phys. Soc. Jpn. **65**, 1949 (1996).
[23] Y. Iino and M. Imada, J. Phys. Soc. Jpn. **65**, 3728 (1996).
[24] M. Imada and Y. Iino, J. Phys. Soc. Jpn. **66**, 568 (1997).
[25] H.-J. Mikeska, U. Neugebauer, and U. Schollwöck, Phys. Rev. B **55**, 2955 (1997).
[26] A. W. Sandvik, E. Dagotto, and D. J. Scalapino, Phys. Rev. B **56**, 11701 (1997).
[27] T. Miyazaki, M. Troyer, M. Ogata, K. Ueda, and D. Yoshioka, J. Phys. Soc. Jpn. **66**, 2580 (1997).
[28] G. B. Martins, M. Laukamp, J. Riera, and E. Dagotto, Phys. Rev. Lett. **78**, 3563 (1997).
[29] M. Laukamp, G. B. Martins, C. Gazza, A. L. Malvezzi, E. Dagotto, P. M. Hansen, A. C. López, and J. Riera, Phys. Rev. B **57**, 10755 (1998).
[30] M. Greven and R. J. Birgeneau, Phys. Rev. Lett. **81**, 1945 (1998).
[31] M. Arlego, W. Brenig, D. C. Cabra, F. Heidrich-Meisner, A. Honecker, and G. Rossini, Phys. Rev. B **70**, 014436 (2004).
[32] F. Anfuso and S. Eggert, Europhys. Lett. **73**, 271 (2006).
[33] K. Trinh, S. Haas, R. Yu, and T. Roscilde, Phys. Rev. B **85**, 035134 (2012).
[34] F. Tedoldi, R. Santachiara, and M. Horvatić, Phys. Rev. Lett. **83**, 412 (1999).
[35] J. Das, A. V. Mahajan, J. Bobroff, H. Alloul, F. Alet, and E. S. Sørensen, Phys. Rev. B **69**, 144404 (2004).

[36]S. Imai, T. Masuda, T. Matsuoka, and K. Uchinokura, arXiv:cond-mat/0402595.
[37]M. Hase, I. Terasaki, and K. Uchinokura, Phys. Rev. Lett. **70**, 3651 (1993).
[38]H. Fukuyama, T. Tanimoto, and M. Saito, J. Phys. Soc. Jpn. **65**, 1182 (1996).
[39]K. Manabe, H. Ishimoto, N. Koide, Y. Sasago, and K. Uchinokura, Phys. Rev. B **58**, R575 (1998).
[40]B. Grenier, J.-P. Renard, P. Veillet, C. Paulsen, G. Dhalenne, and A. Revcolevschi, Phys. Rev. B **58**, 8202 (1998).
[41]D. Augier, E. Sørensen, J. Riera, and D. Poilblanc, Phys. Rev. B **60**, 1075 (1999).
[42]D. G. Shelton and A. M. Tsvelik, Phys. Rev. B **57**, 14242 (1998).
[43]B. Normand and F. Mila, Phys. Rev. B **65**, 104411 (2002).
[44]N. Laflorencie, D. Poilblanc, and A. W. Sandvik, Phys. Rev. B **69**, 212412 (2004).
[45]N. Laflorencie, D. Poilblanc, and M. Sigrist, Phys. Rev. B **71**, 212403 (2005).
[46]J. Bobroff, N. Laflorencie, L. K. Alexander, A. V. Mahajan, B. Koteswararao, and P. Mendels, Phys. Rev. Lett. **103**, 047201 (2009).
[47]A. Dobry, P. Hansen, J. Riera, D. Augier, and D. Poilblanc, Phys. Rev. B **60**, 4065 (1999).
[48]N. Laflorencie and D. Poilblanc, Phys. Rev. Lett. **90**, 157202 (2003).
[49]E. C. Andrade and M. Vojta, Europhys. Lett. **97**, 37007 (2012).
[50]O. Mentré, E. Janod, P. Rabu, M. Hennion, F. Leclercq-Hugeux, J. Kang, C. Lee, M.-H. Whangbo, and S. Petit, Phys. Rev. B **80**, 180413 (2009).
[51]A. A. Tsirlin, I. Rousochatzakis, D. Kasinathan, O. Janson, R. Nath, F. Weickert, C. Geibel, A. M. Läuchli, and H. Rosner, Phys. Rev. B **82**, 144426 (2010).
[52]L. K. Alexander, J. Bobroff, A. V. Mahajan, B. Koteswararao, N. Laflorencie, and F. Alet, Phys. Rev. B **81**, 054438 (2010).
[53]A. Lavarélo, G. Roux, and N. Laflorencie, Phys. Rev. B **84**, 144407 (2011).
[54]T. Sugimoto, M. Mori, T. Tohyama, and S. Maekawa, Phys. Rev. B **87**, 155143 (2013).
[55]K. W. Plumb, Z. Yamani, M. Matsuda, G. J. Shu, B. Koteswararao, F. C. Chou, and Y.-J. Kim, Phys. Rev. B **88**, 024402 (2013).
[56]K.-Y. Choi, J. W. Hwang, P. Lemmens, D. Wulferding, G. J. Shu, and F. C. Chou, Phys. Rev. Lett. **110**, 117204 (2013).
[57]A. Furusaki, M. Sigrist, P. A. Lee, K. Tanaka, and N. Nagaosa, Phys. Rev. Lett. **73**, 2622 (1994).
[58]A. Furusaki, M. Sigrist, E. Westerberg, P. A. Lee, K. B. Tanaka, and N. Nagaosa, Phys. Rev. B **52**, 15930 (1995).
[59]E. Westerberg, A. Furusaki, M. Sigrist, and P. A. Lee, Phys. Rev. B **55**, 12578 (1997).
[60]B. Frischmuth and M. Sigrist, Phys. Rev. Lett. **79**, 147 (1997).
[61]B. Frischmuth, M. Sigrist, B. Ammon, and M. Troyer, Phys. Rev. B **60**, 3388 (1999).
[62]T. Hikihara, A. Furusaki, and M. Sigrist, Phys. Rev. B **60**, 12116 (1999).
[63]E. Yusuf and K. Yang, Phys. Rev. B **67**, 144409 (2003).
[64]J. A. Hoyos and E. Miranda, Phys. Rev. B **69**, 214411 (2004).
[65]T. Giamarchi, C. Rüegg, and O. Tchernyshyov, Nat. Phys. **4**, 198 (2008).
[66]I. Affleck, Phys. Rev. B **43**, 3215 (1991).
[67]T. Giamarchi and A. M. Tsvelik, Phys. Rev. B **59**, 11398 (1999).
[68]D. S. Petrov, M. Holzmann, and G. V. Shlyapnikov, Phys. Rev. Lett. **84**, 2551 (2000).
[69]S. Dettmer, D. Hellweg, P. Ryytty, J. J. Arlt, W. Ertmer, K. Sengstock, D. S. Petrov, G. V. Shlyapnikov, H. Kreutzmann, L. Santos, and M. Lewenstein, Phys. Rev. Lett. **87**, 160406 (2001).
[70]T. Nikuni, M. Oshikawa, A. Oosawa, and H. Tanaka, Phys. Rev. Lett. **84**, 5868 (2000).
[71]C. Rüegg, N. Cavadini, A. Furrer, H.-U. Güdel, K. Krämer, H. Mutka, A. Wildes, K. Habicht, and P. Vorderwisch, Nature (London) **423**, 62 (2003).
[72]M. Jaime, V. F. Correa, N. Harrison, C. D. Batista, N. Kawashima, Y. Kazuma, G. A. Jorge, R. Stein, I. Heinmaa, S. A. Zvyagin, Y. Sasago, and K. Uchinokura, Phys. Rev. Lett. **93**, 087203 (2004).
[73]V. S. Zapf, D. Zocco, B. R. Hansen, M. Jaime, N. Harrison, C. D. Batista, M. Kenzelmann, C. Niedermayer, A. Lacerda, and A. Paduan-Filho, Phys. Rev. Lett. **96**, 077204 (2006).
[74]M. Klanjšek, H. Mayaffre, C. Berthier, M. Horvatić, B. Chiari, O. Piovesana, P. Bouillot, C. Kollath, E. Orignac, R. Citro, and T. Giamarchi, Phys. Rev. Lett. **101**, 137207 (2008).
[75]C. Rüegg, K. Kiefer, B. Thielemann, D. F. McMorrow, V. Zapf, B. Normand, M. B. Zvonarev, P. Bouillot, C. Kollath, T. Giamarchi, S. Capponi, D. Poilblanc, D. Biner, and K. W. Krämer, Phys. Rev. Lett. **101**, 247202 (2008).
[76]B. Thielemann, C. Rüegg, K. Kiefer, H. M. Rønnow, B. Normand, P. Bouillot, C. Kollath, E. Orignac, R. Citro, T. Giamarchi, A. M. Läuchli, D. Biner, K. W. Krämer, F. Wolff-Fabris, V. S. Zapf, M. Jaime, J. Stahn, N. B. Christensen, B. Grenier, D. F. McMorrow, and J. Mesot, Phys. Rev. B **79**, 020408 (2009).
[77]T. Hong, A. Zheludev, H. Manaka, and L.-P. Regnault, Phys. Rev. B **81**, 060410 (2010).
[78]R. Yu, L. Yin, N. S. Sullivan, J. S. Xia, C. Huan, A. Paduan-Filho, N. F. Oliveira, Jr., S. Haas, A. Steppke, C. F. Miclea, F. Weickert, R. Movshovich, E.-D. Mun, B. L. Scott, V. S. Zapf, and T. Roscilde, Nature (London) **489**, 379 (2012).
[79]A. Zheludev and T. Roscilde, arXiv:1305.1194.
[80]G. Roux, A. Minguzzi, and T. Roscilde, New J. Phys. **15**, 055003 (2013).
[81]M. Vojta, Phys. Rev. Lett. **111**, 097202 (2013).
[82]J. P. Álvarez Zúñiga and N. Laflorencie, Phys. Rev. Lett. **111**, 160403 (2013).
[83]H.-J. Mikeska, A. Ghosh, and A. K. Kolezhuk, Phys. Rev. Lett. **93**, 217204 (2004).
[84]T. Roscilde, Phys. Rev. B **74**, 144418 (2006).
[85]R. Yu, S. Haas, and T. Roscilde, Europhys. Lett. **89**, 10009 (2010).
[86]R. Yu, O. Nohadani, S. Haas, and T. Roscilde, Phys. Rev. B **82**, 134437 (2010).
[87]T. Vekua and A. Honecker, Phys. Rev. B **73**, 214427 (2006).
[88]S. R. White, Phys. Rev. Lett. **69**, 2863 (1992); Phys. Rev. B **48**, 10345 (1993); U. Schollwöck, Rev. Mod. Phys. **77**, 259 (2005).
[89]A. W. Sandvik and J. Kurkijärvi, Phys. Rev. B **43**, 5950 (1991); A. W. Sandvik, *ibid.* **59**, 14157 (1999); O. F. Syljuåsen and A. W. Sandvik, Phys. Rev. E **66**, 046701 (2002); H. G. Evertz, Adv. Phys. **52**, 1 (2003).
[90]J. Sirker, N. Laflorencie, S. Fujimoto, S. Eggert, and I. Affleck, Phys. Rev. Lett. **98**, 137205 (2007).
[91]C. Payen, E. Janod, K. Schoumacker, C. D. Batista, K. Hallberg, and A. A. Aligia, Phys. Rev. B **62**, 2998 (2000).

[92]G. Xu, J. F. DiTusa, T. Ito, K. Oka, H. Takagi, C. Broholm, and G. Aeppli, Phys. Rev. B **54**, R6827 (1996).
[93]A. Lavarélo and G. Roux, Phys. Rev. Lett. **110**, 087204 (2013).
[94]F. Casola, T. Shiroka, A. Feiguin, S. Wang, M. S. Grbić, M. Horvatić, S. Krämer, S. Mukhopadhyay, K. Conder, C. Berthier, H.-R. Ott, H. M. Rønnow, C. Rüegg, and J. Mesot, Phys. Rev. Lett. **110**, 187201 (2013).
[95]F. Bert, S. Nakamae, F. Ladieu, D. L'Hôte, P. Bonville, F. Duc, J.-C. Trombe, and P. Mendels, Phys. Rev. B **76**, 132411 (2007).
[96]S. R. White and I. Affleck, Phys. Rev. B **54**, 9862 (1996).